TÉCNICO LISBOA

Path Planning and Fiber Angle Optimization of Continuous Fiber Composites for Additive Manufacturing

Mariana Manuel Martins das Neves de Pinho Fernandes

Thesis to obtain the Master of Science Degree in

Aerospace Engineering

Supervisor: Prof. Afzal Suleman

Examination Committee

Chairperson: Prof. Fernando José Parracho Lau

Supervisor: Prof. Afzal Suleman

Member of the Committee: Prof. José Arnaldo Pereira Leite Miranda Guedes

December 2019

To my sisters, Joana and Adriana, who inspired me to write this thesis but will never read it.

Acknowledgments

My first words must go to my supervisor, Doctor Afzal Suleman, for the wonderful learning experience I lived at University of Victoria, in Canada.

A heartfelt thank you to Abdolrasoul Sohouli, for patiently walking me through the early stages of the theme and getting me up to speed. His help and constant availability are seen by me as a genuine gesture of friendship.

Then, I would like to thank the team at CfAR, Mário, Luís, Ricardo, Martin, Peter, João, Beatriz, Ramalho and Pablo, for the great working environment and for the endless jokes and adventures. An extra thank you for João and Mário, for being my TeamViewer's support team.

I would also like to thank Jack for the amazing times, for teaching me a new word everyday and for always cheering me up with Minky and Lynx pictures.

Even though I spent the past 6 months away from home and with an 8 hour time difference, my friends in Portugal always had my back and it felt like I have never left. Sofia, Inês, Humberto, Samuel, Rita, Mariana and Ana Maria, thank you for your endless friendship and for being there for me.

Thank you Jordina, for the endless audios and for keeping up with me, whenever and wherever we are.

A special note for Ana, who has been with me since day one of this adventure and who will always be the best one cheering me up. Thank you for always making me see the bright side of life.

Ana, Vicente, Maria, Dinis e Manel, thank you for being my home away from home.

Finally, words will always do a poor job at expressing how much I am grateful to my parents, grandparents and my sisters. Thank you very much for always supporting me and for being my fans. Los quiero.

Resumo

Desde os seus primórdios, a indústria aeroespacial tem como principais objetivos melhorar o desempenho e a eficiência das aeronaves. Questões económicas, energéticas e, mais recentemente, ambientais tornaram-me motores críticos do design de aeronaves. Desta forma, materiais mais leves e resistentes, que por sua vez resultam numa diminuição do consumo de combustível, são um dos principais tópicos de pesquisa na indústria.

Neste sentido, tecnologias de fabricação aditiva têm sido implementadas numa série de aplicações. Modelagem de Deposição Fundida, uma das técnicas mais populares, é o método de producão de termoplásticos mais utilizado com fins de prototipagem, cujas principais vantagens são o custo reduzido, o desperdício quase inexistente e a facilidade de mudanaça de material. Dadas as limitações no que diz respeito a propriedades mecânicas, surge a ideia de adicionar materiais de reforço, tais como fibras de carbono. Surgem assim os compósitos reforçados com fibra de carbono.

Por outro lado, recentes desenvolvimentos nas tecnologias de fabricação aditiva levaram ao aparecimento de novas técnicas de design que vão para além das técnicas convencionais. Estes desenvolvimentos levaram ao aparecimento de soluções inovadores e mais eficientes como os compósitos de ângulo variável, que permitem explorar e tirar melhor partido das fibras curvilineas, ainda que isso também resulte em mais dificuldades no que ao processo de produção diz respeito.

Os principais objetivos desta tese são implementar um algoritmo de *path planning* e otimizar o tempo de impressão e a resistência da peça, recorrendo ao algoritm genético disponibilizado pelo MATLAB, para fibras lineares e curvas.

Palavras-Chave: Fabricação Aditiva, Modelagem de Deposição Fundida, Compósitos de Ângulo Variável, *Path Planning*, Algoritmo Genético.

Abstract

Since its early days, the aerospace industry has aimed to improve aircraft performance and efficiency. Economic, energetic and, most recently, environmental issues have become critical design drivers. Therefore, lighter and stiffer materials, which lead to less fuel consumption, are one of the most important research topics in the industry.

In this line of thought, Additive Manufacturing (AM) technologies have been successfully implemented in a series of applications. Fused Deposition Modeling (FDM), one of the most popular AM techniques, is a method for fabricating thermoplastic parts, used as rapid prototyping with advantages of low cost, minimal waste and ease of material change. Due to the intrinsically limited mechanical properties, the idea of adding reinforced materials (such as carbon fibers) into plastic materials to form thermoplastic matrix carbon fiber reinforced plastic (CFRP) composites emerges.

Furthermore, the recent developments in AM technologies lead to the emergence of new design techniques which go beyond the classical design rules, thus leading the designer to find innovative and more efficient solutions like the variable angle-tow (VAT) composites. VAT composites allow taking advantage from the benefits related to the curvilinear fibre path in the most effective way, though their utilisation unavoidably implies an increased complexity of the design process.

The main goal of this thesis is to implement a path planning algorithm and optimize both the printing time and the stiffness of the produced part, making use of the MATLAB Genetic Algorithm, for curved and straight fibers.

Keywords: Additive Manufacturing, Fused Deposition Modeling, Carbon Fiber Reinforced Plastic, Variable Angle-Tow Composites, Path Planning, Genetic Algorithm.

Contents

List of Tables

List of Figures

Acronyms

ABS Acrylonitrile Butadiene Styrene

AFP Automated Fibre Placement

AM Additive Manufacturing

CAD Computer Aided Design

CFF Continuous Filament Fabrication

DLP Direct Light Projection

EBM Electron Beam Melting

FDM Fused Deposition Modelling

FEA Finite Element Analysis

FFF Fused Filament Fabrication

GA Genetic Algorithm

GUI Graphical User Interface

LENS Laser Engineered Net Shaping

LOM Laminated Object Manufacturing

PA Polyamide

PC Polycarbonate

PLA Polyactide

PPSF Polyphenylsulfone

RP Rapid Prototyping

SLA Stereo Lithography

SLM Selective Laser Melting

SLS Selective Laster Sintering

Chapter 1

Introduction

The purpose of this chapter is to state the background and objectives of the thesis, and to describe the basic tools used in this work.

First, motivations are explained. This discussion is followed by a general overview of the topics of this study as well as the main objectives. Finally, the chapter ends with an outline of the chapters to be further presented.

1.1 Motivation

Additive Manufacturing (AM) processes allow a higher degree of freedom when compared to traditional manufacturing methods. This technology enables the production of complex surfaces and internal structures that can translate into parts that present greater structural loads at lower masses. These properties are particularly interesting for the aerospace industry, since the smallest mass reduction can yield a significant fuel cost reduction over the lifetime of a vehicle [1].

While current computer-aided design (CAD) tools allow the design of geometries with complex features, the manual optimization of the mechanical properties of a structure can be exhausting [2]. The manual process would require the engineer to propose a design, analyze its performance using Finite Element Analaysis (FEA) and finally make the revisions based on the results to improve the performance of the design. Even after several trial-and-errors iterations of the process, the final product can still be a suboptimal, since the surfaces and topologies available for production using AM are nearly infinitely variable.

Laminated parts built using Fused Deposition Modelling (FDM) are becoming increasingly popular. However, these parts, normally made of thermoplastic polymers, lack strength and stiffness, restricting their application. In fact, when analyzing the composition of each layer of a part printed using this technology, a different approach should be used. In FDM, the thin thermoplastics rasters are analyzed as ”reinforcement” of a ”matrix” of void space, being the voids the empty spaces in between rasters and layers [3]. The existence of void is the main reason for the low mechanical properties of FDM printed parts.

Therefore, there is a critical need to improve the strength of FDM-fabricated pure thermoplastic parts to overcome these limitations. One of the possible methods is adding reinforced materials (such as carbon fibers) into plastic materials to form thermoplastic matrix carbon fiber reinforced plastic (CFRP) composites [4].

However, in order to produce composite parts by FDM with specific characteristics, it is essential to achieve models for the FDM material mechanical properties. As a matter of fact, to predict their behaviour for different load cases is one the of the main goals in the micromechanics field. This prediction is based in each component's relevant properties and also the geometry and how the constituents of the composite part are interrelated.

As part of this goal, this work aims to develop an optimization framework capable of determining the best fiber type (straight or curved) and also the best fiber orientation, that leads to the best result when both the printing time and the strain (or stress) are considered.

Optimization with Genetic Algorithm (GA) provides a way to bypass much of manual iteration. In order to navigate a vast and dynamic design space, the dynamics of biological evolution suggest ways of continuously expanding the design space towards new and unexplored possibilities [5]. This Genetic Optimization is able to take the boundary conditions, loading, performance targets and objectives as inputs, and output an optimal structure for whichever chosen object.

GA has been used in several researches for composite optimization in recent years, and it has been revealed as a good optimizer in this field [6][7][8].

To the best knowledge of the author, there is no study for the integration of the structural optimization with the path planning of continuous fiber reinforced composite structures. However, these structures have been topic of research for a while. Another critical objective that should be considered during the optimization process is the printing time of a given structure. The main goal of the additive manufacturing industry is to be side by side the traditional industry, and in a fast and continuously changing world, the speed of the processes is of great importance.

1.2 Objectives and Overview

The objective of this work is the development of an optimization framework for the continuous Fibre-reinforced composite structures to maximize the structural performance and minimize printing time with the minimum number of cuts during the placement, using additive manufacturing. To this end, a path planning should be developed to determine the position of the fibers during the optimization process. The fibers can be placed based on a straight or curved paths. Hence, two types of path are employed to fill the design domain. The optimization objectives are the printing time and the structural performance, which can be analyzed based in stress or strain. The optimization solver is GA and the structural analysis is evaluated using a Finite Element (FE) Software, Abaqus.

Details on the path planning and also on the computation of the printing time will be provided over the next chapters. When it comes to the structural part, several python scripts were written in order to perform the FEA in Abaqus, for different cases. The optimization process requires the link between

MATLAB and Abaqus, and the most appropriate way to do it is through a Python Script. The framework will also be further explained along this thesis. Finally, the genetic Algorithm is implemented, and for every case study the best structure will be determined.

The tasks undertaken during the execution of the thesis are hereby summarized in chronological order:

1. Implementation of the continuous path planning algorithm and computation of the printing time;
2. Determination of the material properties of the carbon fibers and matrix used in the process of FDM;
3. Development of the Python Scripts in order to conduct the FEA;
4. Implementation of the genetic algorithm using MATLAB;
5. Development of a multi-objective optimization based on GA.

1.3 Thesis Outline

The following list the contents to be introduced and discussed in each of the chapters of this thesis.

- Chapter 1 (Introduction) - A brief description of the framework, motivation and the objectives of the work are carried out.
- Chapter 2 (State of the Art) - In this chapter a general overview of AM processes, current challenges and barriers and also the different applications in the aerospace industry are outlined. Within the AM methods, FDM is highlighted and methods are described in order to improve the mechanical properties of the final parts, including the addition of fiber reinforcement, in particular continuous fiber reinforcement. Moreover, a description of the work done so far in Variable-Angle Tow composites, in path planning for AM and in structural optimization using GA is done.
- Chapter 3 (Numerical Modelling: Methodology) - An outline of the optimization framework is carried out, the choice of the Finite Element (FE) software is justified, as well as the different simulation strategies. Furthermore, the pre-processing using Python Scripts is also explained. Finally, an outline of the Genetic Algorithm and its implementation in MATLAB is made.
- Chapter 4 (Background) - In this chapter, the mechanical properties of the printed parts are determined, the mathematical model to define curved fibers and also the definition of the equations used to determine the mechanical properties for each element are explained.
- Chapter 5 (Implementation) - Once the theory is all outlined, this chapter presents all the implementation done in order to perform the optimization, from the material definition in Abaqus to the definition of the objective functions fot the GA. The printing technology is also briefly approached and it emerges as an introduction for the path planning algortihm, for both straight and curved

fibers. As a complement, the determination of printing time is also explained and the chapter ends with a study of mesh convergence.

- Chapter 6 (Results) - In the beginning of this chapter the different case studies are introduced, and then the results are presented, compared and discussed, for the different geometries and optimization methods.
- Chapter 7 (Conclusion and Future Work) - The conclusions are presented as well as suggestions for future work.

Chapter 2

State of the Art

The chapter proceeds with an overview of AM, and its importance in the aerospace industry. The technology of Fused Deposition Modelling will be given more importance since it is the technology behind the straight fibers implementation. The chapter ends with an overview of VAT composites, path planning for AM processes.

2.1 Additive Manufacturing

Additive Manufacturing, which emerged under the name Rapid Prototyping (RP), is a process of joining materials to make objects from 3D model data, usually layer upon layer [ASTM F2792 [9]]. This technology has been rapidly developed in the past few years. According to the Wohlers Report 2018 [10], there was an overall industry growth of 21%, which is translated in more than $1.25 Billion dollars.

This development is due to the well and widely recognized advantages of AM. Regarding the aerospace industry, complex additive manufacturing processes must be developed to meet the industry's stringent requirements and to ensure that the products can achieve the established performance levels [11]. Furthermore, companies like Boeing, aware of the fact that AM enables an efficient design process which can achieve innovative design solutions, have introduced this technology in their engineering model, being the SES-15 spacecraft the first significant application of additive manufacturing [12].

Since 2009, the ASTM International Standards Worldwide subcommittee F42.91 [13] has decided that all layered, additive processing methods now fall under the category of Additive Manufacturing. Stereo Lithography (SLA) and Laminated Object Manufacturing (LOM) are the earliest AM techonologies and their products could only be used as prototypes, given the weak structural strength. Nowadays, the Additive Manufacturing technologies have matured into a palette of technologies that yield structurally strong parts with high dimensional accuracy. Especially Selective Laser Melting (SLM), succeeding the Selective Laster Sintering (SLS) technology, as well as Stereo Lithography (SLA) and its derivative, Direct Light Projection (DLP), are processes suitable for producing parts of a quality that allow for the processes to be integrated in production chains [14].

Various materials such as metals, ceramics, polymers and biomaterials are applied in the AM indus-

try. Mainly due to the cheap price and simple fabrication, polymers are the most prevalent materials for AM [15]. Bettina Wendel et al. [16] provided a comprehensive overview of AM methods for polymers and their applications. Most common additive processing techniques for polymers are SLA, SLS, LOM, FDM. FDM is one of the most important AM technologies, and it is going to be explored in greater detail in subsection 2.1.3.1.

Regardless of the specific Additive Manufacturing processes, it is important to point out that all the processes share several similarities, such as being based upon adding material to a workpiece starting from an empty build-surface, being layered process methods and being numerically controlled. The following schematic 2.1 is introduced in order to understand the common grounds between each process:

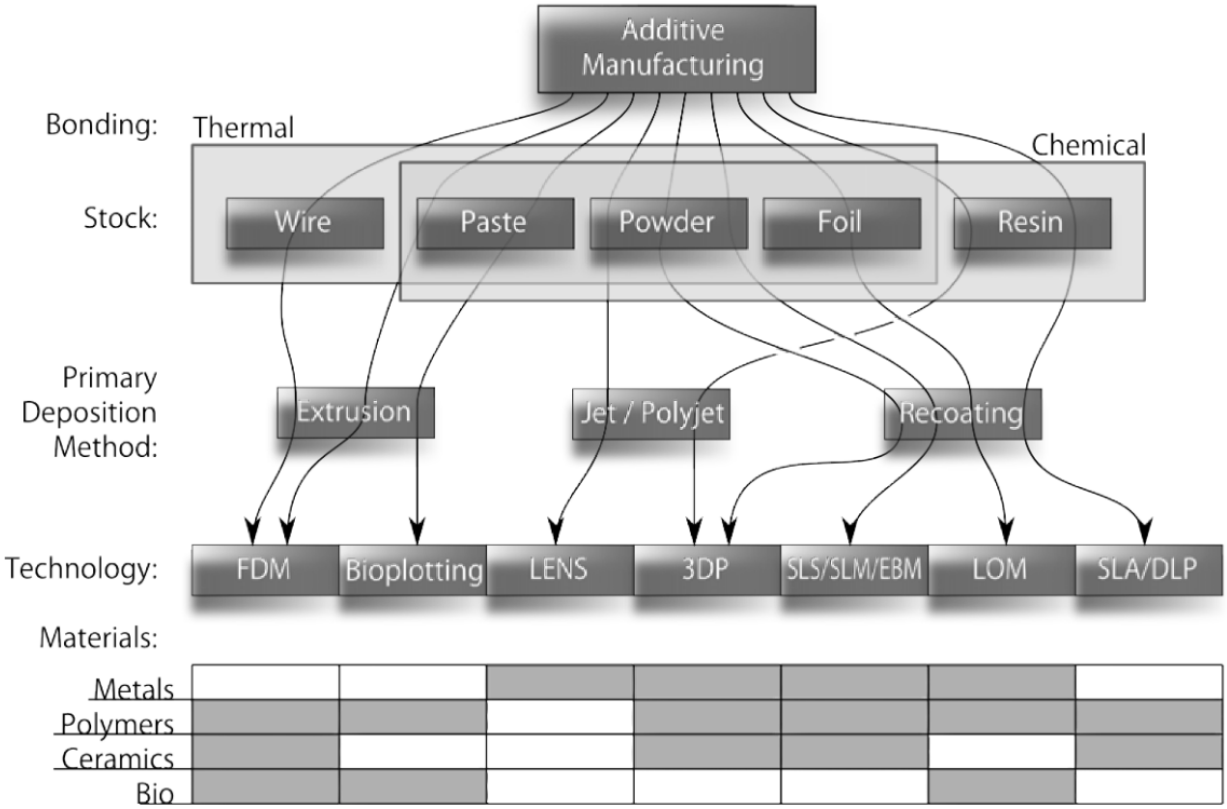

Figure 2.1: AM Process Branches [14]

The pallete of AM can be initially organized in two main categories, related to how the material is bonded to a structure. The bonding can either be Thermal, if the technology uses a thermal process to additively form the structures, or Chemical, if a chemical process is used.

Regarding the stock material, there are five types taken into account: Wire-feed; paste; powder; foil and photo-initiated resins. When it comes to the primary deposition method, there are three differents types to consider: Point-wise extrusion; Point-wise or multi-point ejection from a jet or a polyjet system; Coating/Re-coating the entire build plane with a powder or a photo-initiated resin.

In the next level of the technology, the specific technologies are listed, and also what materials they operate with: Fused Deposition Modelling allows for extrusion of thermo-polymers, ceramics, thermo-

polymers based composites and biological material; Bioplotting allows the deposition of biological material in a similar fashion to FDM; Laser Engineered Net Shaping (LENS) allows selectively spray-coating of metals; Selective Laser Sintering, Melting & Electron Beam Melting (EBM) allow for sintering or melting of a powder, either thermoplastic, metal or ceramic, in a powder-bed; Laminated Object Manufacturing allows for contour tracing and layered manufacturing of metal, polymer and paper foil; Stereo Lithography & Direct Light Projection allow for selective curing of photo-initiated polymer resins and composites with ceramic fillers.

Before moving on to a deeper understanding of the AM technology, it is important to add one more layer to the previous schematic, which are the categories in which each process is inserted. According to [9], AM processes can be categorized into seven categories: Vat photo-polymerization; Material jetting; Binder jetting; Material extrusion; Powder bed fusion; Sheet lamination, Directed energy deposition.

The table in figure 2.2 sums up the most important characteristics of each process.

CATEGORIES	TECHNOLOGIES	PRINTED "INK"	POWER SOURCE	STRENGTHS / DOWNSIDES
Material Extrusion	Fused Deposition Modeling (FDM)	Thermoplastics, Ceramic slurries, Metal pastes	Thermal Energy	• Inexpensive extrusion machine • Multi-material printing • Limited part resolution • Poor surface finish
	Contour Crafting			
Powder Bed Fusion	Selective Laser Sintering (SLS)	Polyamides /Polymer	High-powered Laser Beam	• High Accuracy and Details • Fully dense parts • High specific strength & stiffness • Powder handling & recycling • Support and anchor structure • Fully dense parts • High specific strength and stiffness
	Direct Metal Laser Sintering (DMLS)	Atomized metal powder (17-4 PH stainless steel, cobalt chromium, titanium Ti6Al-4V), ceramic powder		
	Selective Laser Melting (SLM)			
	Electron Beam Melting (EBM)		Electron Beam	
Vat Photopolymerization	Stereolithography (SLA)	Photopolymer, Ceramics (alumina, zirconia, PZT)	Ultraviolet Laser	• High building speed • Good part resolution • Overcuring, scanned line shape • High cost for supplies and materials
Material Jetting	Polyjet / Inkjet Printing	Photopolymer, Wax	Thermal Energy / Photocuring	• Multi-material printing • High surface finish • Low-strength material
Binder Jetting	Indirect Inkjet Printing (Binder 3DP)	Polymer Powder (Plaster, Resin), Ceramic powder, Metal powder	Thermal Energy	• Full-color objects printing • Require infiltration during post-processing • Wide material selection • High porosites on finished parts
Sheet Lamination	Laminated Object Manufacturing (LOM)	Plastic Film, Metallic Sheet, Ceramic Tape	Laser Beam	• High surface finish • Low material, machine, process cost • Decubing issues
Directed Energy Deposition	Laser Engineered Net Shaping (LENS) Electronic Beam Welding (EBW)	Molten metal powder	Laser Beam	• Repair of damaged / worn parts • Functionally graded material printing • Require post-processing machine

Figure 2.2: Classification of additive manufacturing processes by ASTM International [17]

In the case of material extrusion, as shown in table 2.2, there are several process parameters that influence the final part strength, quality, cost and production time, including (but not limited to): **Material and support selection**, **Part design**, **Layer thickness**, **Print design (wall thickness, infill pattern)**, **Print conditions (uniformity of extruder and/or build-bed temperature)**, **Presence of re-enforcing**

material (e.g. carbon fibers).

2.1.1 A comparative overview of AM

As previously mentioned, the growing success of AM technologies is mostly justified by its unique capabilities, listed below:

Flexibility of Design The distinctive feature of AM technologies is the layer-wise fabrication approach, which enables the creation of a wide range of complex geometry shapes. The few constraints imposed by the processes, allow a designer to selectively place (multi-)material precisely where is it needed to attain the desired functionality. This flexibility emerges in contrast to subtractive processes, who demand fixtures and diverse tooling, and carry a great possibility of collisions and difficulties in reaching deeper zones [18]. Further design constraints are imposed by other traditional manufacturing processes, including formative techniques (e.g., pressing, casting).

Cost of geometric complexity AM allows geometric complexity at no further cost. Moreover, there is no need for extra tooling. Even though complexity is possible to achieve with other processes, this comes with a cost increase.

Printing Tolerance Print tolerance, or dimensional accuracy, determines the deviation of the finished model, when compared to the original CAD. When the technology was still in an early stage the main goal was prototyping, so there was not a concern to distinguish resolution and accuracy. However, given the growing expectations into delivering finished products, the need of establishing accuracy standards arises.

Need for Assemblage This technology allows the production of parts, which would otherwise require assembly of several parts, if manufactured conventionally.

Time and cost efficiency in production run Even though conventional processes are cost and time effective, the start-up cost is still high. When comparing to AM processes, these are significantly slower, but better suited for low quantity production, since there is almost no initial investment. Furthermore, on-demand and on-location AM can lower inventory costs and potential reduce costs related to supply chain and delivery. When it comes to material waste, it is practically non-existent, resulting in a very low 'buy-to-fly' ratio for AM.

2.1.2 AM applications in the aerospace industry

Using Additive Manufacturing for prototyping is a common practice within the aerospace industry, however, only recently has this technology been used to produce end use parts. Besides the develop-

ment of the method itself, the main reason is the high requirements that need to be met in order to get the necessary approval from the regulatory agencies [20].

Additive manufacturing can be applied to rapid prototyping, rapid tooling, and/or rapid manufacturing. Rapid prototyping is used in order to quickly produce a prototype of a part from the CAD file, at the design phase [21]. When it comes to rapid tooling and manufacturing, these belong to the manufacturing phase. Rapid tooling is used to make a tool for injection molding or die casting operations [22], on the other hand, rapid manufacturing is used to produce end use parts [23]. All the three categories are covered in the industry and summed up in table 2.1.

Table 2.1: The classification of 3D printing applications in the aircraft industry [24]

Category	Applications
Rapid Prototyping	• To test the functional spare parts of vehicles,engines, or platforms; • To generate the prototypes of aircraft parts; • To evaluate the machinability of molds made with silicon matrices.
Rapid Tooling	• To make the molding model of turbocharger blades and impellers; • To mimic natural structures in making aircraft part; • To identify the truss lattice with optimal elastic performance for UAV wing design.
Rapid Manufacturing	• To make spare parts for aircraft maintenance; • To make an entire drone or UAV; • To create a global supply chain of spare parts.

Current 3D printing practices in the aircraft industry were observed from the following perspectives: adoption by major manufacturers, market for 3D printing applications and 3D printing applications for aircraft maintenance.

2.1.2.1 Adoption by majors manufacturers

The increasing use of Additive Manufacturing by major manufacturers backs up the importance and prevalence of 3D printing applications in the aircraft industry. Next, a benchmark on some of the publically available information from the aerospace industry will be presented:

- **Airbus** - Both engine parts and internal cabin parts are typical products of 3D printing technologies. Furthermore, the currently available technology can produce all parts required to construct an aircraft that meets high quality standards.
- **Boeing** - In space systems alone, a small team is delivering nearly 1,000 additively manufactured parts to flight programs [25]. The company notes that it can save up to 30% when using 3D printing when compared to traditional manufacturing [26].
- **European Space Agency (ESA)** - ESA has collaborated with the AM machine manufacturer 3D Systems on metal AM. The conventional design of their injector, combustion chamber and expansion nozzle have been 3D printed. They have also investigated benefits of redesigning the

components for AM. The flow in the injector could be optimised and made into one component instead of five. [27].

- **General Electrics (GE)** - A first metal fuel nozzle to be made by 3D printing was proposed by GE [28]. GE opened a 3D printing factory for the nozzles in Auburn, Alabama, and the first LEAP-powered Airbus A320neo started ferrying paying passengers in the summer of 2017 [29].

2.1.2.2 Market for 3D printing applications

Whereas software and services currently contribute a small share of the revenues, it was estimated that within 4 years, the proportions of hardware and materials will decline to half of the total revenues, and the share of software and relevant services will dramatically increase [24]. The markets for 3D printing software, services, and spare parts are expected to nearly triple.

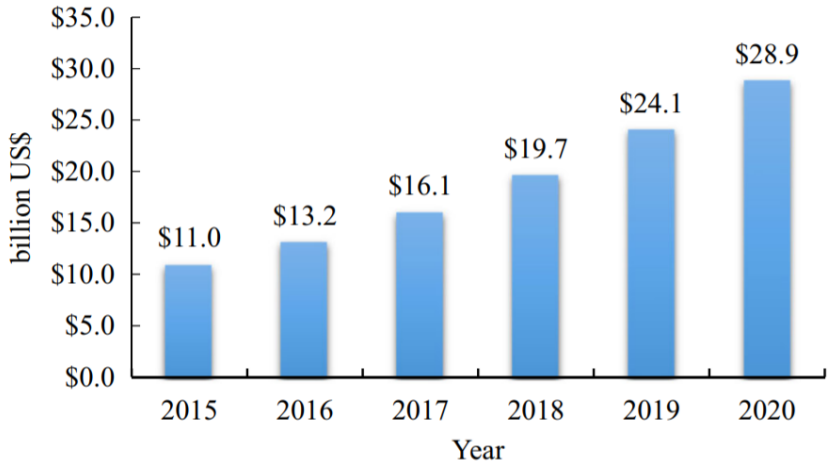

Figure 2.3: 2015–2020 3D printing markets [24]

2.1.2.3 3D printing applications for aircraft maintenance

AM has been applied to produce spare parts for some components, where the engine is the most critical. These spare parts are easily damaged, which is inconvenient for imported spare parts that require constant replacement.

Starting in 2013, spare parts have been 3D printed, and table 2.2 shows different examples. For companies that demand small quantities of spare parts for engine maintenance, 3D printing technologies can lower production costs and shorten maintenance cycles.

Table 2.2: Companies that use 3D printing technologies [24]

Company	Name of Spare Parts	Remark
Rolls-Royce Group plc	Metal spare parts of jet engines	Trial production since 2013
Siemens	Metal spare parts of gas turbines	Applicable since 2014
Honeywell	Heat exchangers and metal stents	Trial production since 2013
MTU Aero Engines AG	Blade components of high press guides with complex shapes	Applicable since 2018
General Electric Company	Spare parts of the fuel nozzles of engines in Boeing 747 and Airbus 320	Applicable since 2016

2.1.3 Additive Manufacturing Techniques of Composite Structures

Developments of new manufacturing techniques of composite structures, being AM one of the most important, allow the designer to go beyond standard designs, meaning that there is the possibility to find innovative and more efficient results.

First, an overview of Fused Deposition Modelling and the state of the art of the technology will be explored. Then, the Variable Angle-Tow composites will be approached.

2.1.3.1 Fused Deposition Modelling (FDM)

Fused Deposition Modeling is the numerically controlled additive fabrication of structures by thermoplastic extrusion from a material deposition unit. The pocess was invented by Steven Scott Crump and published in 1992 under a US patent [30].

In this mechanism, a STL file is loaded into a slicing software or into the specific machine-computer interface platform. Then, the file is loaded in the FDM machine and it starts printing the part according to the pre defined settings. Once the process is finished, the part can be removed from the platform and post-processes, if needed.

The machine itself consists in two miniature extruder head nozzles, one for the modeling material and the other for the cases an overhanging section has to be produced. This overhanging features can be described as any feature that does not have a support under it to hold it to the model. In these cases, a removable support has to be printed by the second nozzle. After the completion of the part, this support can be removed either manually (simple geometries) or chemically (deep cavities or places with difficult access) [31]. Two schemes are introduced below in figure 2.4.

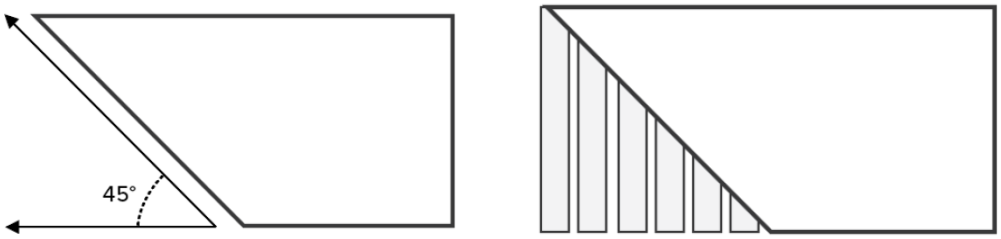

(a) Overhang of more than 45 degrees; No support needed

(b) Overhang of less than 45 degrees: support needed

Figure 2.4: Overhanging features [32]

As shown in figure 2.5, in FDM processes, parts are fabricated by extruding a filament through a temperature controlled heat nozzle, in a pattern onto a platform [33].

As the material is deposited, it cools, solidifies and bonds with the adjoining material. As the layer is completed, the build platform moves downward the length corresponding to one layer thickness, in order to carry on with the process for the next layer. These steps will be repeated until the part is completed [33].

The filament used is generally 1.75mm in diameter. The nozzle is positioned at the end of the extrusion mechanism, and it is kept at a constant temperature in order to assure a correct flow of the

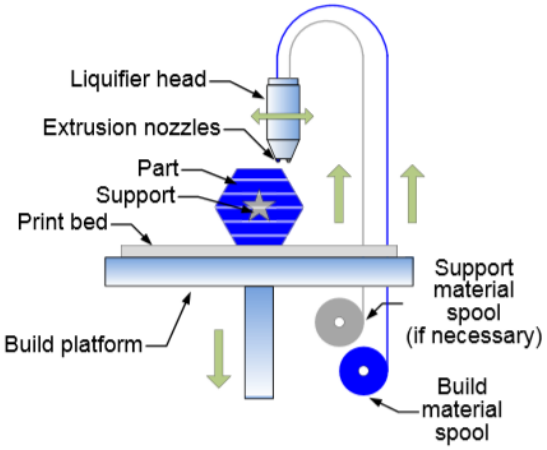

Figure 2.5: Schematic of FDM processes [33]

material. The nozzles control the diameter of the filament flowing through the extruder and it usually ranges between 0.1 and 1mm [34]. The nozzle is directly connected to the liquifier output, which means the specifications, i.e., process temperature, high thermal condutivity, are similar [35].

The build platform is another essential part of the system, since it is where the part is deposited. Being so, the role of this component is to provide a flat surface with good adhesion properties, in order to ensure the first layers are fixed for the duration of the printing process, but at the same time, not too fixed, so that the part can be removed in the end.

Finally, another critical issue is the temperature control. If the temperature is not controlled, thermal gradients develop along the part through both the cross section and the height, resulting in warping the part during the process [36]. The most common solution is to maintain the building platform at a high temperature, between 70-90^{o}C [37].

Regarding the materials currently used in this technology, the most common are: acrylonitrile butadiene styrene (ABS), polycarbonate (PC), polylactide (PLA), polyamide (PA), polyphenylsulfoen (PPSF) and the mixture of any two types of thermoplastic materials [38][39]. Given the weak structure associated to the parts produced using FDM, the main application is usually conceptual prototypes with mature development stages.

As mentioned before, in order to improve the strength of the produced parts, reinforced materials (such as carbon fibers) are added into plastic materials forming thermoplastic matrix carbon fiber reinforced plastic composites. In CFRP composites, the carbon fibers can be used to support the load, meanwhile the matrix can be used to bind and protect the fibers and transfer the load to the reenforcing fibers.

2.1.3.2 State of the Art in FDM composites

Even though FDM has been around for several years, its application to fiber reinforced thermoplastic composites is still recent, translating into a limited number of studies regarding the matter. Fiber reinforcement in thermoplastics has three forms: short, long and continuous fibers. The criteria used to differentiate the three forms is the length of the fibers. Long fibers present a fiber length of 1-25mm

while, on the other end, short fibers are 0.5mm in length or less. Continuous fibers are used in high performance composites and its length can be the size of the full composite itself. Some studies have shown that, in general, mechanical properties improve with increasing fiber length [40][41].

Since the main goal of the reinforcement is to take full advantage of the possible enhancement of the mechanical properties, it is important to assure a good interfacial bonding, so that the reinforcement can receive the loads that stress the composite to its breaking point. If the bonding is not assured and the reinforcement does no take the loads, the part will fail at an inferior load than it was supposed to, and the fibers will pull out of the matrix, without breaking [42]. Considering that the load is transferred from the matrix to the fibers by shear forces acting on their surface, it is important that its surface is higher than their cross-sectional area, i.e., have a high aspect ratio. Long fibers (and continuous fibers, obviously), therefore, reinforce more efficiently than short fibers or particles since they have a higher aspect ratio. The second reason why continuous fibers usually prevail in the reinforcements processes it is because it is possible to control its orientation precisely. Meaning, the internal structure of the composite can be designed to anticipate the stress it will face, improving its efficiency. And this is exactly part of the goal of this thesis.

The AM of continuous fiber reinforced thermoplastic composites has been a very active research area in the past few years, and it is a better fit for the aerospace and automotive industries, since it allows a higher fiber orientation control and can provide better directional properties to the parts. In this process, both the thermoplastic and continuous fiber are fed simultaneously into the nozzle. Next, a selection of studies regarding continuous fibers was carried out and will be explained briefly throughout the next paragraphs.

Matsuzaki et al. [43] came up with a new method for 3D printing of CFRP composites using FDM, where PLA and continuous fibers were supplied separately to the nozzle. Both carbon and jute fibers were used. Tensile and flexural tests were performed and the results, when compared to pure PLA samples showed a significant improvement in the properties of the fiber reinforced PLA. However, the strength of Jute reinforced fibers was not as significant due to the loss of fiber-matrix interactions.

Klift et al. [44] tested the capabilities of Mark One 3D printer, the first commercial 3D printer capable of printing continuous fibers composites. The material used was Nylon reinforced with carbon fibers. There were three different types of samples printed, with 10 layers each: the first sample was pure Nylon; the second sample had two carbon fiber layers in the middle and the third sample had six layers of fiber in the middle. The tensile test was performed in order to evaluate the mechanical properties and to make sure the rule of mixtures of composites was met. Both specimens reinforced with carbon fibers verified an improvement of the mechanical properties, however, the discontinuities in the fibers led to the non confirmation of the rule of mixtures.

Li et al. [45] introduced a method in order to solve the flaw present in the results of Matsuzaki et al. [43]. The same matrix and fibers were used, but instead, a conical nozzle was used to produce uniform mixing of resin and fiber. There was some pre processing in order to improve the adhesion between the carbon fibers and PLA. The tests were done on pure PLA samples, carbon reinforced PLA samples and modified carbon fiber reinforced PLA samples. The results stated that the modified carbon fiber

reinforced PLA samples showed considerably higher flexural strength as compared to original samples of reinforced carbon fiber, proving the effectiveness of pre processing.

Nakagawa et al. [46] proposed a new method to produce continuous carbon fiber composites. The material used was ABS reinforced with carbon fibers. In this study, two nozzles with different diameters were used, in order to realize the impact of it. Instead of printed coaxially, the fibers were sandwiched between upper and lower layers of ABS. In order to bond the ABS and the fibers both a heating pin and a microwave were used. An improvement in the mechanical properties was verified and there was not much of a difference between the specimen thermally bounded by heating pin and microwave oven.

Vaneker et al. [47] described a pultrusion based method using PP as the matrix and E-glass as reinforcement, where a cutting device was incorporated and a new deposition strategy was implemented. The results shows an increase in flexural modulus when compared to pure PP. However, the existent voids were a major issue in the process.

Yamawaki et al. [48] developed a new 3D printer for CFRP composites with two different extruders, one to supply the matrix, Nylon, and the other the fiber, carbon fiber. The composite samples of 2, 3 and 4 layers were printed with an extrusion temperature of 250° C, a feed rate of 60 mm/min, and a volume fraction of 50%. The samples were post-processed using annealing and hot press treatment to observe the effect in mechanical properties. The tensile tests showed the hot press treatment led to an improvement on the tensile strength and Young's modulus of the specimen. On the other hand, annealing had a marginal effect on mechanical properties.

2.1.3.3 Variable Angle-Tow (VAT) Composites

Lightness is a fundamental requirement to be met in the aerospace industry, and this characteristic keeps pushing towards the development of new materials. Composites are an example of material with a high stiffness-to-weight and strength-to-weight ratios, which leads to a phenomenal weight-saving. And even though composites have been around for a while now, emerging AM techniques like automated fiber placement (AFP) or the continuous tow shearing (CTS), allow to go further from the traditional design rules, leading the design away from the classical straight fibers format.

The emergence of these technologies led to the creation of a new class of composite materials: the variable angle-tow composites, as modern AM machines allows the placement of the fibers along a curvilinear path, which implies a point-wise variation of the material properties. Associated with the innumerous design possibilities, there is also the complexity of the design process, which emerges due to two properties of VAT composites: the heterogeneity and the anisotropy, that intervene at different scales and that vary point-wise over the structure [49]. Furthermore, another difficulty associated with the technique is due the printing technology itself, which could introduce differences between the numerical model and the real structure, such as imperfections.

In this process, fibers are aligned to the reference tow path because of the head rotation, even when the steered tow paths are simply shifted along a specific direction (shifting direction), which inevitably leads to tow gaps or overlaps [50]. Besides, another limitation of the modelling is that the angle variation must be represented by a numerical equation. This constraint causes difficulty in modelling when it is

not possible to find simple numerical expressions for the designed tow paths or when multiple different tow paths are defined within a ply [51]. In this thesis, the results are only based in the AFP process, so there is effectively an equation that describes the placement of the fiber and it is explained in subsection 4.2.2.

Up until this point, there are not a lot of research done with VAT composites, and no general rules or methods were developed in order to obtain an optimum design [52]. When it comes to the technology itself, the most suitable available in the market at the moment is the Markforged Mark Two Industrial Strength® 3D Printer. This printer is equiped with a dual head system with a Continuous Filamente Fabrication (CFF) print head and an Fused Filament Fabrication (FFF) extrusion head.

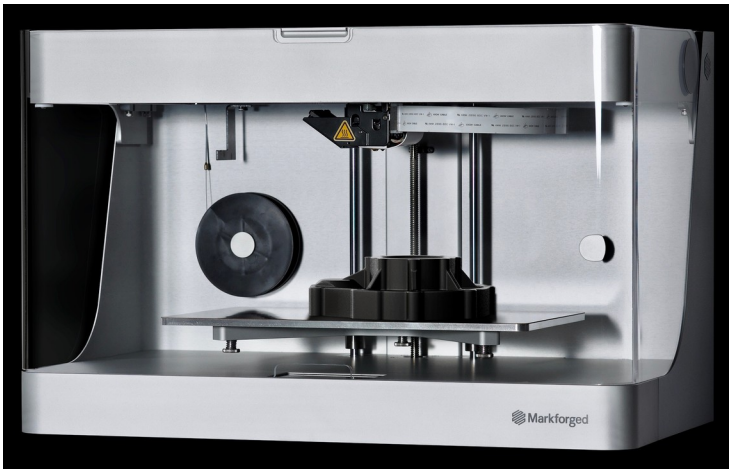

Figure 2.6: Markforged Mark Two Industrial Strength® 3D Printer

A brief explanation of the basic function of the printer will be given. One should notice that the validation of the optimised configurations through the fabrication of prototypes is beyond the scope of this thesis.

The Mark Two uses a dual head system with a FFF extrusion head combined with a CFF print head to reinforce 3D printed nylon-based components with carbon. Furthermore, the fiber nozzle includes also a cutting system to cut the fiber at the end of the path.

What distinguished this printer from other 3D printers and Rapid Prototyping machines for composites is the fact that the fiber reinforcement is continuous, which is proven that improves the mechanical properties of the structure [49], as previously explained. .

The Mark Two 3D printer is one of the most advanced 3D printers, and the main advantage of this model is the capability of printing with two different materials for the matrix and up to four types of continuous fibers: Carbon Fiber, Fiberglass, Kevlar and HSHT Fiberglass (High-Strength High-Temperature Fiberglass).

2.2 Path Planning for Additive Manufacturing Processes

The first step into preparing the printing process is the slicing process, that even though will no be implemented in this work, had to be mentioned, since it is one of the most important steps. There are

two types of slicing: Unidirectional Slicing and Multidirection Slicing.

Another crucial step in AM is the development of an elaborate path planning strategy. Different technologies demand different accuracy and materials. Methods used to generate different types of deposition paths are listed and briefly explained.

- Raster Path Planning
  - Raster Path (Figure 2.7a)): 2D regions are filled by a set of scan lines with finite width [54]. It is commonly employed in commercial AM systems due to its simple implementation;
  - Zig-Zag Path (Figure 2.7b)): It emerges deriving from raster path, combining the separate parallel lines into a single continuous pass, which reduces the number of tool-path passes. The outline accuracy of both approaches is poor due to the discretization errors on any edge that is not parallel to the tool motion direction [53].
  - Contour Path (Figure 2.7c)): Li et al. [45] developed an optimal tool-path patterns for sculptured parts with a single island and no seriously non-convex shape.
  - Spiral Path (Figure 2.7d)): Specially used in numerically controlled (NC) machining [63], it can also be used to solve the problems of zigzag tool paths in AM process, but is only suitable for certain special geometrical models.
  - Hybrid Path (Figure 2.7e)): The hybrid path planning strategy is promising as it shares some merits of various approaches [53]. A combination of contour and zigzag pattern leads to the satisfaction of both geometrical and build efficiency conditios. Zhang et al. [55] came up with a new approach which inlcudes and outline vector, which allows the maintenance of surface quality and accuracy, and an inner zigzag path which is faster and more universal.
- Continuous Path Planning
  - Hilbert Filling Curve (Figure 2.8a)): is a continuous path, which can cover a region of space without intersecting itself, developed by Bertoldi et al. [56]. However, the countless turns needed are not suitable for AM.
  - Fractal Path Planning (Figure 2.8b)): This method, first introduced by Wasser et al. [57], decomposes the area to be filled in nodes, and the number of nodes depends on the pretended accuracy. However, for large areas and high accuracy, the processing time required would be unacceptably long. Moreover, highly convoluted paths may result in accumulation of heat in certain regions, therefore inducing excessive distortion of the part [53].

2.3 Structural Optimization via Genetic Algorithms (GA)

To achieve the optimum design is obviously the main goal for any designer. This ”optimum design” is the one which minimized the objective function initially defined. There is a tendency of defining cost based objective functions, however, the best structure is not necessarily the cheapest, which means that

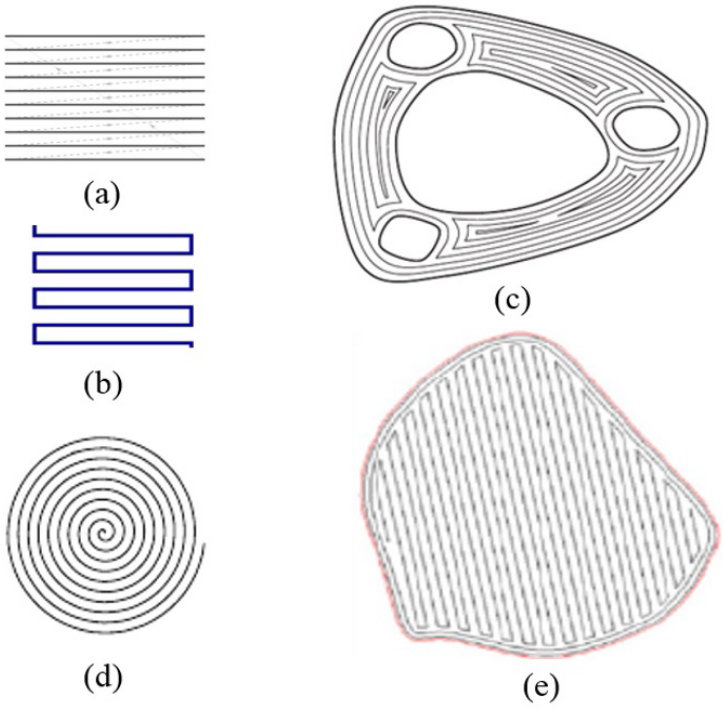

Figure 2.7: Raster Path Pattern [53]

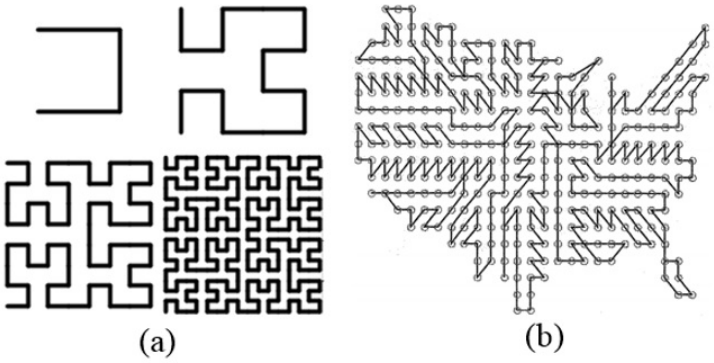

Figure 2.8: Continuous Path Pattern [53]

other objectives may sometimes be more important and conveniently used in studies in optimum design [58].

David Gilbert (University of Illinois), in the middle 80s, managed to successfully applied genetic algorithms to structural optimization for the first time [59]. When compared to other optimization methods, genetic algorithms have the capacity to approach different problems from different perspectives simultaneously, being possible to optimize both the geometry and the topology. This fact emerges as a great advantage when compared to the other evolutionary methods.

In general, structural design is required to conform to a number of inequality constraints related to stress, deflection and other variables. In the genetic algorithm these are conveniently handled by a 'penalty'. The levels of penalties imposed can be 'tuned' so that minor infringements suffer small penalties whereas major violations lead to their elimination from the process.

Several works where GAs were applied to the design of composite structures can be found in the

literature, and here two will be mentioned: Martín et al. [60] performed the geometric design of the composite materials of a stiffened panel using a genetic algorithm and static analysis, and considering hydrothermal effects. Nagendra et al. [61] with the goal of decreasing the computational cost involved in the design of composite panels, also made use of GAs.

In general, GAs were shown to be one of most reliable tools in optimization problems [62].

When compared to gradient based optimization techniques, this is where GA is different:

1. No gradient information is required, only the fitness value is required;
2. GA does not move sequentially from one point to the next one, but many new points are evaluated during the iteration. The GA convergence is controlled by few parameters: the population size (Ps), the probability of crossover (Pc) and the probability of mutation (Pm).

Chapter 3

Numerical Modelling: Methodology

In this chapter, the methodology adopted to model both the straight and the curved fibers process is presented. First, the framework will be outlined, as an introduction so it is easier to understand both the FEA and the GA optimization and how are they connected. Then, the selection of the Finite Element simulation software is discussed. This is followed by a discussion of the key process models that will be used to implement the placement of the fibers in the path planning. Finally, the pre- and post- processing parts of the simulation are presented.

The last part of the chapter will be devoted to the explanation of the theory behind the genetic algorithm.

3.1 Outline of the Optimization Process

The outline of the work is presented in this section. A flowchart presented in Figure 3.1 represents an overview of this thesis work in terms of activities. The different colors in the flowchart were introduced in order to differentiate the software where the actions take place: the first two blocks actions are performed in MATLAB, while the last block action is performed in Abaqus.

The whole process of optimization starts with the assignment of a random angle (or angles, for the case of the curved fibers), which will lead to the initial design. This initial design is plotted using a MATLAB code which is based in a path planning algorithm. From this initial design, two different variables are obtained:

- Printing Time - Obtained from the MatLab code mentioned above;
- Strain Energy or Stress Von Mises - Obtained from the Finite Element Analysis.

Having computed both variables, the optimization is ready to be run, either it is a strain optimization or a stress optimization (both are explained further in this work). The whole process is repeated until the convergence criteria is achieved.

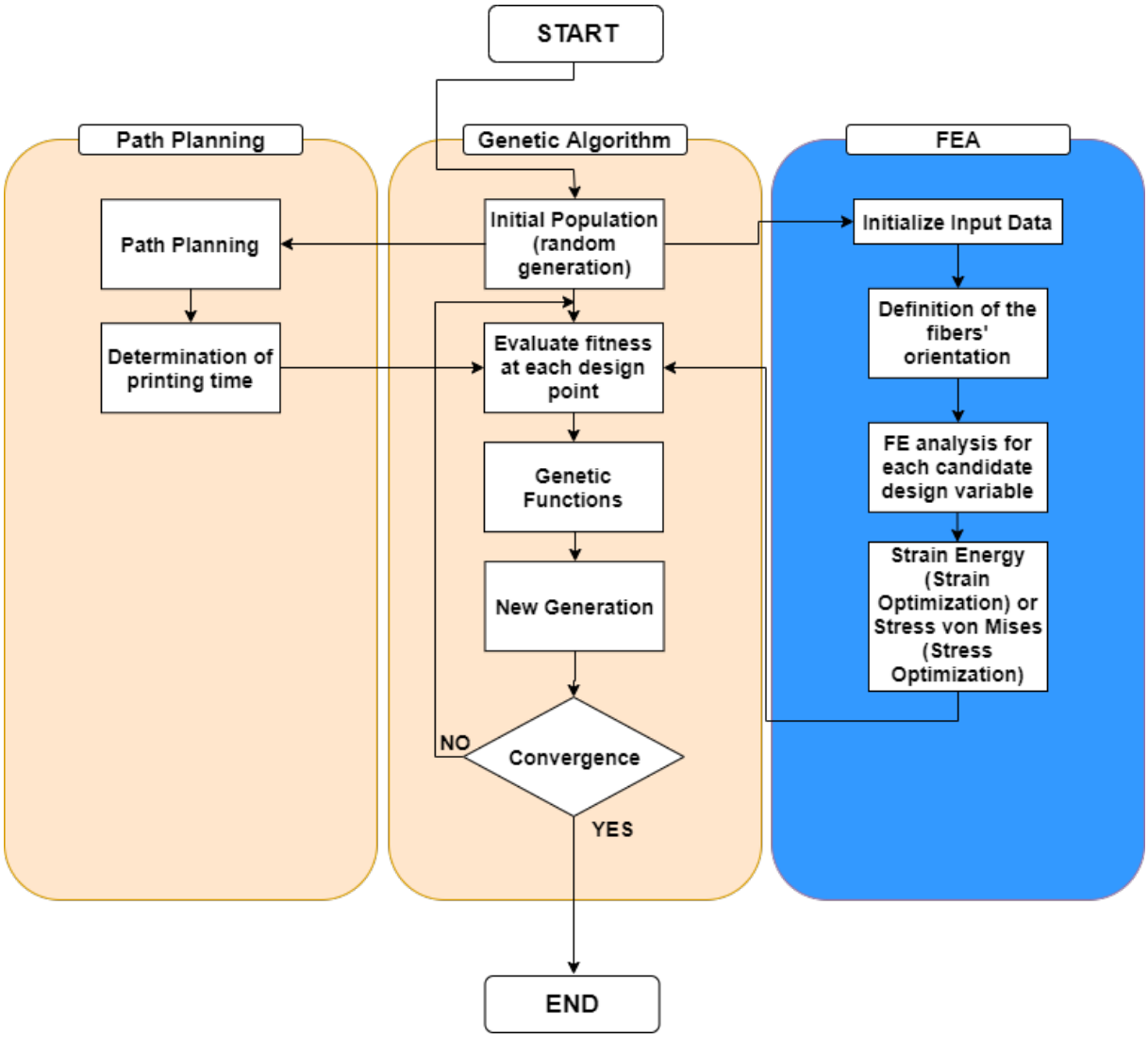

Figure 3.1: Flowchart

3.2 FE Software Selection

To develop the finite element analysis, firstly, a suitable FE simulation software must be selected. For this work Abaqus 6.14.1, from the Dassault systems suite, is chosen as the FE software for simulating the parts. This particular FE software is widely used in the aerospace composites industries due to its reliable and versatile simulation capabilities.

A wide range of simulation strategies are available in this software, and besides, it alows the interlink with other softwares, like MATLAB, in order to compute the printing time.

The software's ability to visualise the FE results is also advantageous to understand the interactions occurring during processing. An in depth modelling of process leads to more realistic predictions of the material response to the process parameters.

3.3 Simulation Strategies

The methodology in achieving the thesis objective is presented in this section. The main reasons to adopt certain simulation strategies are based essentially on the ABAQUS software capabilities. Several simulation strategies were considered, with minimum computational effort while obtaining reliable and accurate results. The selection of modelling strategies were based on analyzing the opportunities available in ABAQUS FE software via its documentation. An extensive explanation of the software's capabilities is published in the ABAQUS Online Documentation [64]. An overview of the simulation strategies adopted is described in the following sections.

3.3.1 ABAQUS/Standard

ABAQUS has two structural analysis types - Standard and Explicit. The ABAQUS/Standard is more appropriate and efficient for solving smooth nonlinear problems; on the other hand, ABAQUS/Explicit is the choice for a wave propagation analysis.

Considering the nature of the process is of a smooth nonlinear characteristic and, moreover, there is no need for a stress wave study, a standard (Implicit) analysis is considered in ABAQUS for this thesis work.

3.3.2 Steady-State Analysis

Once the structural analysis type is defined it is now necessary to decide between steady - state and transient analyses. In a steady state analysis type, the loads applied on the part should be time independent, which is the case. Being so, it is easily concluded that the analysis is steady-state.

3.3.3 Linear Analysis

A linear structural analysis is used when the structure's stiffness does not change during loading, which once again is the case. Having this said, this is the type of analysis performed.

3.3.4 Element Selection

As mentioned before, the majority of the cases to be analyzed are 2D. Asides from the last one which is a 3D model.

The wide range of elements in the ABAQUS element library provides flexibility in modeling different geometries and structures. While for a 2D model the type of element used is the shell element, for a 3D model, continuum (Solid) element type is used. While shell elements approximate a three-dimensional continuum with a surface model, solid elements consist of six faces and eight nodes at the corners.

The fundamental variables that exist at the nodes of an element are the degrees of freedom in the finite element analysis. In this particular thesis, for a stress/displacement simulation, the degrees of freedom are the translations at each node.

Considering the chosen elements for the 2D analysis, a called general-purpose shell element was chosen, S4R. This type of elements provide robust and accurate solutions in all loading conditions for thin and thick shell problems [65].

Regarding the choice of the element for the 3D analysis, the mesh family is of the continuum (Solid) element type. This mesh element consists of six faces and eight nodes at the corners. The degrees of freedom are the fundamental variables calculated during the analysis. For a stress/displacement simulation the degrees of freedom are the translations at each node. The element chosen was C3D8R.

The element's formulation, i.e. the mathematical theory used to define the element's behavior in ABAQUS, is based on the Lagrangian material state. According to this, the material associated with an element remains associated with that element throughout the analysis.

3.4 Pre-Processing: Python Script

Several tasks in Abaqus are time consuming and practically impossible to perform in GUI (Abaqus/CAE). Perform a repetitive task or vary parameters of a simulation as part of an optimization study, which is the case of this thesis, can only be done through Python Scripts [66].

An added advantage to scripting is that the entire analysis is saved in a small readable text file. And it allows to redraw the part, apply the materials, loads, boundary conditions, create the steps, and even create and run the job if programmed to do so. Besides, there is the advantage of readability, since it is not necessary to navigate through the model tree to figure out how the complex geometry was created or how boundary conditions are applied.

In this particular case, one aims to change the orientation of the fibers. Practically, this means that for straight fibers, if using GUI, every time a simulation is to be run, the orientation of the fibers in the Ply have to be changed. For curved fibers, this would mean that for each element a different set of values used to describe the material would have to be computed and applied, and there can be thousands of elements.

Once the python script is finalized, the script is executed in ABAQUS. Instantaneously, an input file is generated based on the script.

The flowchart presented in Figure 3.2 represents the pre-processing in detail along with the flow of the python script.

The material properties and the section assignments are defined in the next step, and it will be explained in further detail in section 4.1. Once the part is meshed and nodes are created, the surface and query sets are defined. The interactions, loads and boundary conditions, once defined, do not change along the simulation process. The final part of the python code is to specify the output requests and to submit the job.

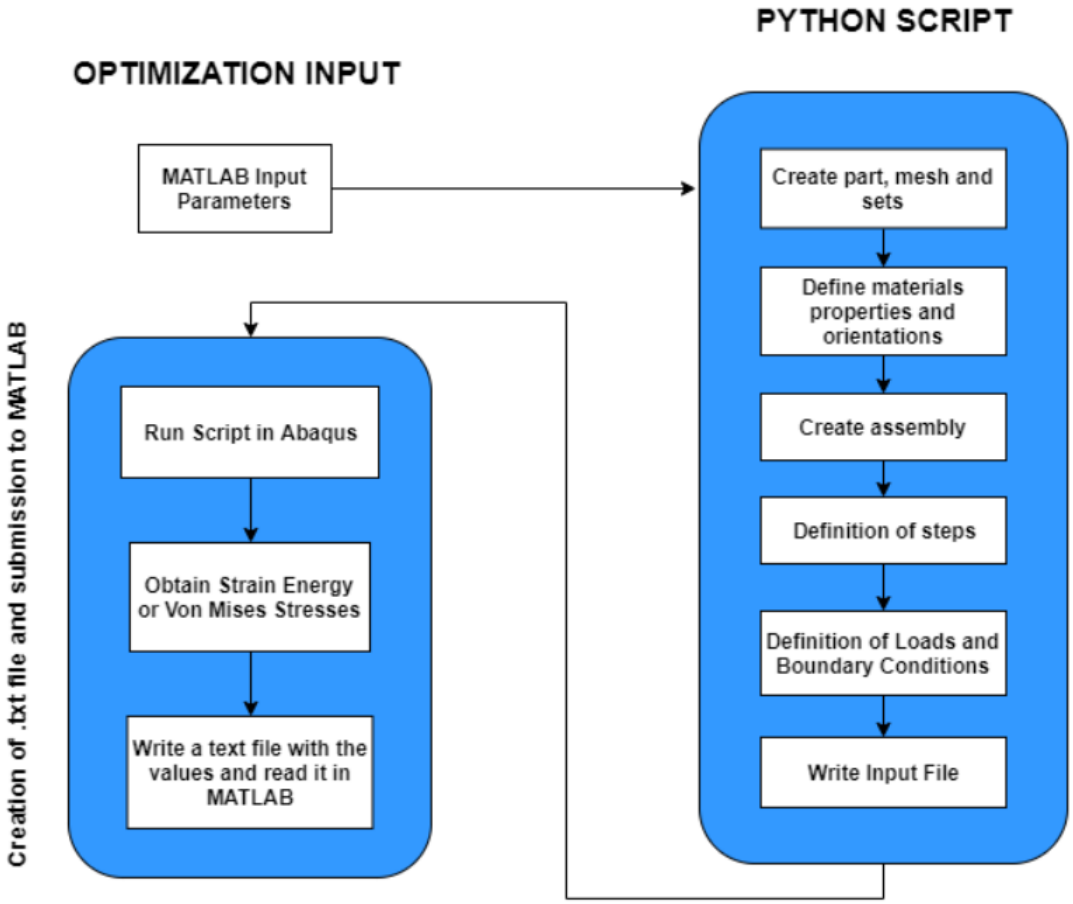

Figure 3.2: Activities of the pre-processing

3.5 Post-Processing

Once the simulation is over, the output files corresponding to Strain Energy or Von Mises Stress, according to the type of optimization performed (Strain Based Optimization or Stress Based optimization, respectively), are read in MATLAB. Since it is one of the variables in the optimization function, it is vital to collect the data coming from ABAQUS in order to proceed with the optimization.

The optimization process will be explained in greater detail in the next section.

3.6 Optimization with Genetic Algorithm

As mentioned before, the optimization algorithm used in this thesis was the Genetic Algorithm (GA). First introduced in the early seventies, it is a stochastic algorithm that mimics the Darwin principles of evolution and has been quite successfully applied in machine learning and optimization problems. The basic unit of these algorithms are populations of individuals, i.e. competing candidate solutions. These individuals are probabilistically modified by genetic operators, such as selection, crossover and mutation, seeking a near-optimal solution to the problem.

The scheme in figure 3.3 represents the basics of the GA algorithm. Contrary to other algorithms, they do not have any additional memory but the current set of individuals in the population. However, in

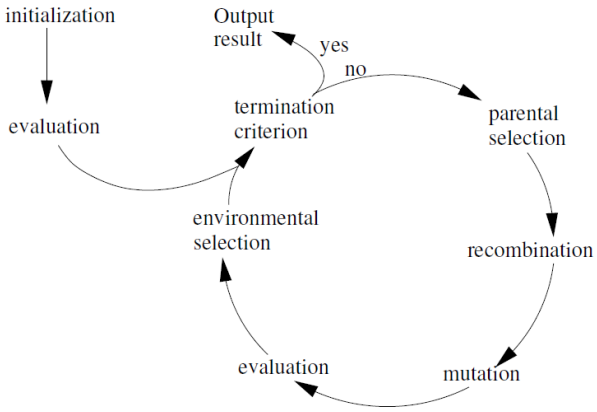

Figure 3.3: Genetic Algorithm [67]

the current work, in order to have a record of the evolution of both the population and the values of the objective functions, the MatLab code was improved.

3.6.1 Coding Strings

In GA, each individual in a population is coded as a fixed-length binary string. The length of the string varies with the domain of the parameters. E.g., if the domain of the parameter x is [-1,1] (which is the case) and the precision requirement is six places after the decimal point, then the domain [-1,1] should be divided into 2,000,000 equal size ranges. The implies that the length of the string requires to be 20, since:

$$524288 = 2^{19} < 1000000 < 2^{20} = 1048576 \tag{3.1}$$

Having this, the decoding from a binary string into a real number is completed in two simple steps:

(1) Convert the binary string $< b_{20}b_{19}...b_0 >$ from base ten:

$$x' = \sum_{i=0}^{19} b_i 2^i \tag{3.2}$$

(2) Calculate the corresponding real number:

$$x = -2.0 + x' \frac{7}{2^{20} - 1} \tag{3.3}$$

3.6.2 Initial Design

The initial population is created, a single value for the case straight fibers and three different values for curved fibers, per patch. Each individual is a binary string with a fixed-length, and every bit of the binary string is randomly initialized.

3.6.3 Evaluation

For every generation, each individual is evaluated against the unknown environment. The fitness values are associated with the values of the objective function.

3.6.4 Genetic Operators

Genetic operators are the drivers of the evolutionary process for the population, following the principle of survival of the fittest. The most widely used genetic operators are reproduction, crossover and mutation [68].

In order to perform these operations, one must select individuals in the population. The strategy used is based on the fitness level of the individuals. There are different strategies based on the fitness, and the most common one is the fitness proportionate selection. Having formed a new population using the mentioned strategy, some members of this new population undergo transformations by means of genetic operators to form new solutions (a recombination step). Due to intuitive similarities, there are only three operators used: reproduction, crossover and mutation.

So it is possible to better understand these operators, a further explanation with some examples will be provided.

The reproduction operator consists simply in, after an individual is selected, copying it from the current population into the new population, without performing any changes.

Regarding the crossover operator, it starts with two selected individuals and the crossover point (an integer between 1 and L-1, where L is the length of strings), is randomly selected. As an example, assuming the two parental individuals are x_1 and x_2 and the crossover point is 5 (L=20). If

$$x_1 = (01001|101100001000101)$$

$$x_2 = (11010|011100000010000)$$

Then the offspring will be:

$$x_1' = (01001|011100000010000)$$

$$x_2' = (11010|101100001000101)$$

Finally, the third operator, mutation, is responsible for inserting random changes in the population, and it may occasionally have beneficial results: escaping from a local optimum.

3.6.5 Genetic Algorithm using MATLAB

In this work, the Genetic Algorithm used will be the Genetic Algorithm Toolbox from MATLAB. This toolbox uses MATLAB matrix functions to build a set of versatile tools for implementing a wide range of genetic algorithm methods. It is a collection of routines, mostly written in m-files, which implement

the most important functions in genetic algorithms. MATLAB supports only one data type, a rectangular matrix of real/complex numeric elements. The main data structures in the GA toolbox are:

- Chromossomes
- Phenotypes
- Objective Function Values
- Fitness Values

Further detail regarding these data structures will be presented in appendix A.

Chapter 4

Background

In this chapter the determination of the mechanical properties of the printed composites and the implementation of curved fibers in *Abaqus* are the covered matters.

4.1 Mechanical Properties of 3D Printed Carbon Fiber Composites

Previously in this work, it was explained the importance of carbon fiber materials for the industry, in particular aerospace, and how 3D printing has enabled companies to print with carbon fiber, albeit with a different binding material than standard carbon fiber processes.

With the ultimate goal of getting results as accurate as possible, the values of layer thickness used in this study are from one of the commercial grade 3D printer capable of printing parts reinforced with continuous fibers such as carbon fiber, Kevlar and fiberglass, the The Mark Two [70].

The previous model, the MarkForged Mark One, was capable of printing continuous fibers only in a concentric nature within the part. The Mark Two printer now has the capability of printing parts in both concentric and isotropic fill types.

Regarding the elastic properties of Nylon, they were computed in a study by Melenka et al [71], except the density, and are presented in the table below (4.1):

Table 4.1: Properties of Nylon Filament

Name	Symbol	Units	Value
Elastic Modulus	E_m	Pa	0.94×10^9
Shear Modulus	G_m	Pa	0.35×10^9
Poissons's Ratio	ν_m	-	0.35
Density [32]	ρ	kgm^{-3}	1100

The carbon fibers properties were computed and obtained from [72], since it required more effort to apply to the Markforged carbon fiber filament. The typical carbon fiber yarn properties were acquired from [72], and are organized in table 4.2.

One should note that the longitudinal elastic modulus listed in the table has been multiplied by the carbon fiber yarn density of 28%, since that the estimated carbon fiber filament volume in the composite

Table 4.2: Assumed material properties of carbon fiber yarn in filament

Name	Symbol	Units	Value
Longitudinal Tensile Modulus	Ef_{11}	Pa	64.7×10^9
Transverse Tensile Modulus	Ef_{22}	Pa	22.4×10^9
Longitudinal Shear Modulus	Gf_{12}	Pa	22.1×10^9
Transverse Shear Modulus	Gf_{23}	Pa	8.3×10^9
Longitudinal Poissons's Ratio	νf_{12}	-	0.30
Transverse Poissons's Ratio	νf_{23}	-	0.35
Density [32]	ρ	kgm^{-3}	1400

includes both carbon fiber yarns and a binding agent, and this fact needs to be corrected [72]. This is because only the carbon fiber yarns are providing any noticeable tensile strength to the composite part. Multiplying the elastic modulus by the yarn density allows this property to be applied to the entire volume of carbon fiber filament.

Finally, the final mechanical properties for the material are obtained using the following equations from micromechanics, where k_m and k_f are the percentage of volume of matrix and fiber, respectively [73]:

$$
\begin{aligned}
&k_m + k_f = 1 \\
&E_{11} = Ef_{11}k_f + E_m k_m \\
&E_{22} = \frac{E_m}{1 - \sqrt{k_f} \times \left(1 - \frac{E_m}{Ef_{22}}\right)} = E_{33} \\
&G_{12} = \frac{G_m}{1 - \sqrt{k_f} \times \left(1 - \frac{G_m}{Gf_{12}}\right)} = G_{13} \\
&G_{23} = \frac{G_m}{1 - \sqrt{k_f} \times \left(1 - \frac{G_m}{Gf_{23}}\right)} \\
&v_{12} = k_f v f_{12} + k_m \nu f_m = v_{13} \\
&v_{23} = \frac{Ef_{22}}{2Gf_{23}} - 1
\end{aligned}
\tag{4.1}
$$

And the final properties of the material, which were computed using a MATLAB code, are summarized in the following table, considering k_f=0.2:

Table 4.3: Properties of the material

Name	Symbol	Units	Value
Longitudinal Tensile Modulus	E_{11}	Pa	18.66×10^9
Transverse Tensile Modulus	E_{22}	Pa	1.535×10^9
Longitudinal Shear Modulus	G_{12}	Pa	0.5863×10^9
Transverse Shear Modulus	E_{23}	Pa	0.5730×10^9
Longitudinal Poissons's Ratio	ν_{12}	-	0.336
Transverse Poissons's Ratio	ν_{23}	-	0.340

4.2 Straight and Curved Fibers

As it was mentioned before, two types of fibers will be considered: straight and curved fibers. When it comes to the implementation of the first case, it is trivial to do so, since the orientation is the same for every fiber and also along the fiber, meaning that it is only necessary to define the orientation of the Composite Layup in *Abaqus*.

Considering the latter case, it is not a as straightforward process as defining the straight fibers because the orientation is changing constantly. Having this, the following sub sections will be devoted to explain the theory needed to implement curved fibers in Abaqus. The implementation itself will be explained in chapter 5.

4.2.1 Material Definition in Abaqus

As part of the optimization process, a Python Script was developed. One of the challenges in the case of the curved fibers was defining the orientation given the fact that, as mentioned in the previous section, it is continually changing.

Having as a starting and common point the properties computed and summarized in table 4.3, two solutions were found and both were implemented:

1. Compute the properties according to the angle of rotation θ of each element and assign them to the element;
2. Define a Composite Layup for each element where the angle is also the angle of rotation θ.

In order to do so, one had to determine the orientation of the fibers in each element, and also determine the properties of the material for that orientation, and the next two sections explain both, respectively.

4.2.2 Functional Fiber Path Representation

Olmedo and G$\ddot{o}$rdal (1993) were the first to introduce a fiber path parameterization scheme in order to study buckling of variable stiffness plates. They define the fiber angles as varying linearly along either the x or y axis, and the authors also demonstrate buckling load improvements of up to 80% with respect to the best straight fibers designs. In 2002, Tatting and G$\ddot{o}$rdal generalized the path definition formulation to vary linearly along and arbitrary axis x', where $\theta(x')$ is defined as:

$$\theta(x') = \phi + (T_1 - T_0)\frac{|x'|}{d} + T_0 \tag{4.2}$$

and T_0 and T_1 are the fiber angles at the beginning and at the end of the characteristic length *d*. Regarding ϕ, it represents the inclination of x' with respect to the global x-axis. Figure 4.1 is presented next in order to clarify the stated idea:

In order to obtain the equation to implement the fibers in MATLAB, the integral of equation 4.2 has to be computed, and the final equation is represented in 4.3:

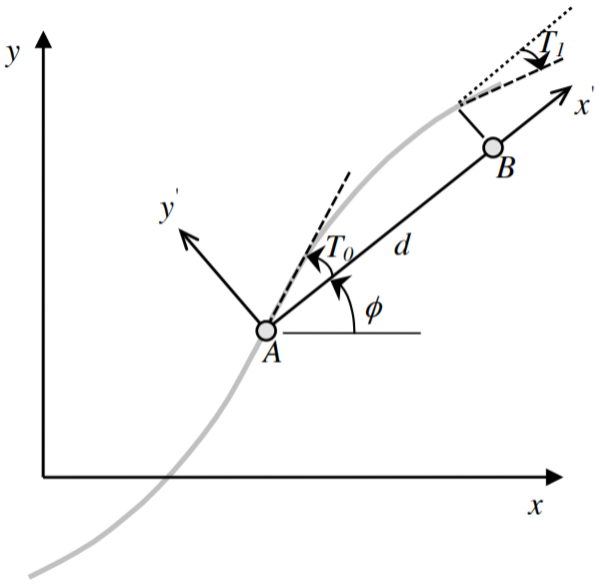

Figure 4.1: Curved Fiber

$$y'(x') = \phi x' + (T_1 - T_0)\frac{|x'|}{2d}x' + T_0 x' \tag{4.3}$$

Once the equation 4.3 is obtained, it is only necessary to define T_0, T_1 and ϕ, in radians.

4.2.3 Constitutive Relations for Orthotropic Materials and Stress-Strain Transformations

Considering an orthotropic material and having computed all the engineering constants along principal directions, it is possible to establish a relation with the compliance coefficients.
If the material is subjected to a 3D state of stress, the resulting strains can be expressed in terms of stress components and engineering constants as follows:

$$\begin{aligned}
\varepsilon_{11} &= \frac{\sigma_{11}}{E_1} - \frac{\nu_{21}}{E_2}\sigma_{22} - \frac{\nu_{31}}{E_3}\sigma_{33} \\
\varepsilon_{22} &= -\frac{\nu_{12}}{E_1}\sigma_{11} + \frac{\sigma_{22}}{E_2} - \frac{\nu_{32}}{E_3}\sigma_{33} \\
\varepsilon_{33} &= -\frac{\nu_{13}}{E_1}\sigma_{11} - \frac{\nu_{23}}{E_2}\sigma_{22} + \frac{\sigma_{22}}{E_2}
\end{aligned} \tag{4.4}$$

and the engineering shear strain components are given as:

$$\begin{aligned}
\gamma_{23} &= \frac{\tau_{23}}{G_{23}} \\
\gamma_{13} &= \frac{\tau_{13}}{G_{13}} \\
\gamma_{12} &= \frac{\tau_{12}}{G_{12}}
\end{aligned} \tag{4.5}$$

where, E_1, E_2 and E_3 are the Young's moduli in 1,2 and 3 directions, respectively. Note that E_1 represent the axial modulus and the axial direction is along the fiber.

G_{ij} represents the shear moduli and it should be noted that $G_{ij} = G_{ji}$.

As it is already known, it is possible to relate strain and stress components through the compliance matrix, whose inverse has the same format as the stiffness matrix, and the relation is written as follows:

$$\begin{bmatrix} \varepsilon_{11} \\ \varepsilon_{22} \\ \varepsilon_{33} \\ \gamma_{23} \\ \gamma_{13} \\ \gamma_{12} \end{bmatrix} = \begin{bmatrix} S_{11} & S_{12} & S_{13} & 0 & 0 & 0 \\ S_{12} & S_{22} & S_{23} & 0 & 0 & 0 \\ S_{13} & S_{23} & S_{33} & 0 & 0 & 0 \\ 0 & 0 & 0 & S_{44} & 0 & 0 \\ 0 & 0 & 0 & 0 & S_{55} & 0 \\ 0 & 0 & 0 & 0 & 0 & S_{66} \end{bmatrix} \begin{bmatrix} \sigma_{11} \\ \sigma_{22} \\ \sigma_{33} \\ \tau_{23} \\ \tau_{13} \\ \tau_{12} \end{bmatrix} \tag{4.6}$$

Combining equations 4.4, 4.5 and 4.6, it is possible to determine the different compliance coefficients in terms of engineering constants:

$$\begin{aligned} S_{11} &= \frac{1}{E_1} & S_{12} &= \frac{-\nu_{21}}{E_2} & S_{13} &= \frac{-\nu_{31}}{E_3} \\ S_{21} &= \frac{\nu_{12}}{E_1} & S_{22} &= \frac{1}{E_2} & S_{23} &= \frac{-\nu_{32}}{E_3} \\ S_{31} &= \frac{\nu_3}{E_1} & S_{32} &= \frac{-\nu_{23}}{E_2} & S_{33} &= \frac{1}{E_3} \\ S_{44} &= \frac{1}{G_{23}} & S_{55} &= \frac{1}{G_{13}} & S_{66} &= \frac{1}{G_{12}} \end{aligned} \tag{4.7}$$

From linear algebra, it is proved that the inverse of a symmetric matrix is also a symmetric matrix. Since the stiffness matrix is symmetric, that leads to the conclusion that the compliance matrix is also symmetric. From this characteristic, it is easy to conclude the following relations:

$$\frac{\nu_{21}}{E_2} = \frac{\nu_{12}}{E_1} \qquad \frac{\nu_{311}}{E_3} = \frac{\nu_{13}}{E_1} \qquad \frac{\nu_{23}}{E_2} = \frac{\nu_{32}}{E_3} \tag{4.8}$$

4.2.4 Stress and Strain Transformation about an axis

As mentioned before, the orientation of the curved fibers will change constantly, so it is necessary to compute the material properties for each θ.

Two notations will be used, the subscripts 123 refer to the principal material directions, while subscripts xyz will refer to the global coordinate directions. A representative scheme of what was explained is introduced in figure 4.2.

In forming flat laminates, fiber-reinforced lamninae are stacked in parallel, but each having its own fiber direction. Considering the z-coordinate is taken along the lamina thickness, the 3 coordinate will always coincide with the z-coordinate.

The relation between the coordinates of a material point in the two coordinates systems is:

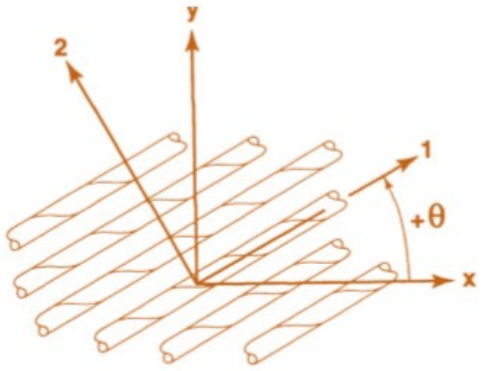

Figure 4.2: Unidirectional lamina with global xyz directions and principal material 123 directions

$$\begin{bmatrix} x_1 \\ x_2 \\ x_3 \end{bmatrix} = \begin{bmatrix} cos\theta & sin\theta & 0 \\ sin\theta & cos\theta & 0 \\ 0 & 0 & 1 \end{bmatrix} \begin{bmatrix} x \\ y \\ z \end{bmatrix} = \Big[L\Big] \begin{bmatrix} x \\ y \\ z \end{bmatrix} \tag{4.9}$$

The inverse of equation 4.9 is

$$\begin{bmatrix} x \\ y \\ z \end{bmatrix} = \begin{bmatrix} cos\theta & -sin\theta & 0 \\ -sin\theta & cos\theta & 0 \\ 0 & 0 & 1 \end{bmatrix} \begin{bmatrix} x_1 \\ x_2 \\ x_3 \end{bmatrix} = \Big[L\Big]^T \begin{bmatrix} x_1 \\ x_2 \\ x_3 \end{bmatrix} \tag{4.10}$$

Important to note that $\Big[L\Big]^{-1} = \Big[L\Big]^T$

The previous transformations are also valid for the unit vectors associated with the two coordinate systems.

$$\begin{bmatrix} \hat{e}_1 \\ \hat{e}_2 \\ \hat{e}_3 \end{bmatrix} = \Big[L\Big] \begin{bmatrix} \hat{e}_x \\ \hat{e}_y \\ \hat{e}_z \end{bmatrix}, \qquad \begin{bmatrix} \hat{e}_x \\ \hat{e}_y \\ \hat{e}_z \end{bmatrix} = \Big[L^T\Big] \begin{bmatrix} \hat{e}_1 \\ \hat{e}_2 \\ \hat{e}_3 \end{bmatrix} \tag{4.11}$$

4.2.4.1 Transformation of Stress Components

Considering now the relationship between the components of stress between both coordinate systems, since stress is a second-order tensor, it transforms according to the formula:

$$\left[\sigma_{kq}\right]_{123} = l_{ki} l_{qj} \left[\sigma_{ij}\right]_{xyz}, \qquad \left[\sigma_{kq}\right]_{xyz} = l_{ik} l_{jq} \left[\sigma_{ij}\right]_{123} \tag{4.12}$$

where $\left[\sigma_{kq}\right]_{123}$ and $\left[\sigma_{kq}\right]_{xyz}$ are the components of the stress tensor in both 123 and xyz coordiante systems, respectively, and l_{ij} are the direction cosines defined by

$$l_{ij} = (\hat{e}_i)_{123} \cdot (\hat{e}_j)_{xyz} \tag{4.13}$$

where $(\hat{e}_i)_{123}$ and $(\hat{e}_j)_{xyz}$ are the orthonormal basis vectors. Equations 4.12 can be expressed in matrix form as:

$$\left[\sigma\right]_{xyz} = \left[L\right] \left[\sigma\right]_{123} \left[L\right]^T, \qquad \left[\sigma\right]_{123} = \left[L\right]^T \left[\sigma\right]_{xyz} \left[L\right] \tag{4.14}$$

Carrying out the matrix multiplications of the second equation 4.14, it is obtained:

$$\begin{bmatrix} \sigma_{xx} \\ \sigma_{yy} \\ \sigma_{zz} \\ \sigma_{yz} \\ \sigma_{xz} \\ \sigma_{xy} \end{bmatrix} = \begin{bmatrix} cos^2\theta & sin^2\theta & 0 & 0 & 0 & -sin2\theta \\ sin^2\theta & cos^2\theta & 0 & 0 & 0 & sin2\theta \\ 0 & 0 & 1 & 0 & 0 & 0 \\ 0 & 0 & 0 & cos\theta & sin\theta & 0 \\ 0 & 0 & 0 & -sin\theta & cos\theta & 0 \\ cos\theta sin\theta & -cos\theta sin\theta & 0 & 0 & 0 & cos^2\theta - sin^2\theta \end{bmatrix} \begin{bmatrix} \sigma_{11} \\ \sigma_{22} \\ \sigma_{33} \\ \sigma_{23} \\ \sigma_{13} \\ \sigma_{12} \end{bmatrix} \tag{4.15}$$

or

$$\left[\sigma\right]_{xyz} = \left[T\right] \left[\sigma\right]_{123} \tag{4.16}$$

For the first equation is, in matrix form, given by:

$$\begin{bmatrix} \sigma_{11} \\ \sigma_{22} \\ \sigma_{33} \\ \sigma_{23} \\ \sigma_{13} \\ \sigma_{12} \end{bmatrix} = \begin{bmatrix} cos^2\theta & sin^2\theta & 0 & 0 & 0 & sin2\theta \\ sin^2\theta & cos^2\theta & 0 & 0 & 0 & -sin2\theta \\ 0 & 0 & 1 & 0 & 0 & 0 \\ 0 & 0 & 0 & cos\theta & -sin\theta & 0 \\ 0 & 0 & 0 & sin\theta & cos\theta & 0 \\ -cos\theta sin\theta & cos\theta sin\theta & 0 & 0 & 0 & cos^2\theta - sin^2\theta \end{bmatrix} \begin{bmatrix} \sigma_{xx} \\ \sigma_{yy} \\ \sigma_{zz} \\ \sigma_{yz} \\ \sigma_{xz} \\ \sigma_{xy} \end{bmatrix} \tag{4.17}$$

or

$$\left[\sigma\right]_{123} = \left[R\right]\left[\sigma\right]_{xyz} \tag{4.18}$$

4.2.4.2 Transformation of Strain Components

Similar to stresses, strains are also second order tensor quantities, and equations 4.16 and 4.18 are valid for tensor components of strains:

$$\left[\varepsilon\right]_{xyz} = \left[L\right]\left[\varepsilon\right]_{123}\left[L\right]^{T} \tag{4.19}$$

$$\left[\varepsilon\right]_{123} = \left[L\right]^{T}\left[\varepsilon\right]_{xyz}\left[L\right] \tag{4.20}$$

Even though previous equations are valid for strain transformations, 4.15 and 4.17 are not valid for single-column formats of strains because of the definition:

$$2\varepsilon_{xy} \quad = \varepsilon_{12} \qquad 2\varepsilon_{xz} \quad = \varepsilon_{13} \qquad 2\varepsilon_{yz} \quad = \varepsilon_{23} \tag{4.21}$$

Taking into consideration this modification:

$$\begin{bmatrix} \varepsilon_{xx} \\ \varepsilon_{yy} \\ \varepsilon_{zz} \\ 2\varepsilon_{yz} \\ 2\varepsilon_{xz} \\ 2\varepsilon_{xy} \end{bmatrix} = \begin{bmatrix} cos^2\theta & sin^2\theta & 0 & 0 & 0 & -sin\theta cos\theta \\ sin^2\theta & cos^2\theta & 0 & 0 & 0 & sin\theta cos\theta \\ 0 & 0 & 1 & 0 & 0 & 0 \\ 0 & 0 & 0 & cos\theta & sin\theta & 0 \\ 0 & 0 & 0 & -sin\theta & cos\theta & 0 \\ sin2\theta & -sin2\theta & 0 & 0 & 0 & cos^2\theta - sin^2\theta \end{bmatrix} \begin{bmatrix} \varepsilon_{11} \\ \varepsilon_{22} \\ \varepsilon_{33} \\ \varepsilon_{23} \\ \varepsilon_{13} \\ \varepsilon_{12} \end{bmatrix} \tag{4.22}$$

$$\begin{bmatrix} \varepsilon_{11} \\ \varepsilon_{22} \\ \varepsilon_{33} \\ \varepsilon_{23} \\ \varepsilon_{13} \\ \varepsilon_{12} \end{bmatrix} = \begin{bmatrix} cos^2\theta & sin^2\theta & 0 & 0 & 0 & sin\theta cos\theta \\ sin^2\theta & cos^2\theta & 0 & 0 & 0 & -sin\theta cos\theta \\ 0 & 0 & 1 & 0 & 0 & 0 \\ 0 & 0 & 0 & cos\theta & -sin\theta & 0 \\ 0 & 0 & 0 & sin\theta & cos\theta & 0 \\ -sin2\theta & sin2\theta & 0 & 0 & 0 & cos^2\theta - sin^2\theta \end{bmatrix} \begin{bmatrix} \varepsilon_{xx} \\ \varepsilon_{yy} \\ \varepsilon_{zz} \\ 2\varepsilon_{yz} \\ 2\varepsilon_{xz} \\ 2\varepsilon_{xy} \end{bmatrix} \tag{4.23}$$

Finally, and similar to the stress transformation:

$$\left[\varepsilon\right]_{xyz} = \left[R\right]^{T}\left[\varepsilon\right]_{123} \qquad \left[\varepsilon\right]_{123} = \left[T\right]^{T}\left[\varepsilon\right]_{xyz} \tag{4.24}$$

4.2.4.3 Transformation of Material Coefficients

The only remaining quantities that need to be computed are the material stiffnesses C_{ij} which are components of a fourth-order tensor, meaning that the tensor transformation law is still applicable. The tensor components C_{ijkl} in the global coordinates can be related to the components C_{mnpq} in the material coordinates by the tensor transformation law

$$\bar{C}_{ijkl} = a_{im}a_{jn}a_{kp}a_{lq}C_{mnpq} \tag{4.25}$$

However, equation 4.25 implies five matrix multiplications. As an alternative, the result can be obtained using equations 4.16, 4.18 and 4.24, resulting in:

$$\{\sigma\}_{xyz} = [T]\{\sigma\}_{123} = [T][C]_{123}\{\varepsilon\}_{123} = [T][C]_{123}[T]^T\{\varepsilon\}_{xyz} \equiv [C]_{xyz}\{\varepsilon\}_{xyz} \tag{4.26}$$

where $[C]_{123}$ is the material stiffness matrix (6×6) in the material coordinates, and $[T]$ is the transformation matrix defined in equation 4.15. Thus the transformed material stiffness matrix is given by:

$$[\bar{C}] = [T][C][T]^T \tag{4.27}$$

where $[\bar{C}] = [C]_{xyz}$ and $[C] = [C]_{123}$. The equation above is valid for general constitutive matrix [C].

In order to relate compliance coefficients in the two coordinate systems, equation 4.24 is used:

$$\{\varepsilon\}_{xyz} = [R]^T\{\varepsilon\}_{123} = [R]^T([S]_{123}\{\varepsilon\}_{123}) = [R]^T[S]_{123}([R]\{\sigma\}_{xyz}) \equiv [S]_{xyz}\{\sigma\}_{xyz} \tag{4.28}$$

Concluding, the coefficients $\bar{S}_{ij}$ (global coordinates) are related to the coefficients S_{ij} (material coordinates) by:

$$[\bar{S}] = [R]^T[S][R] \tag{4.29}$$

The expanded version of equation 4.29 will be introduced in Appendix A.

Chapter 5

Implementation

In this chapter, the material definition in the FE software will be explained. As stated before, there are two approaches: Compute the properties according to the angle of rotation θ of each element and assign them to the element; Define a Composite Layup for each element where the angle is also the angle of rotation θ. The chapter continues with the explanation of the path planning algorithm, as well as the model to compute the printing time, for both curved and straight fibers. Finally, the different optimization methods are explained, and a convergence study is performed.

5.1 Material Definition in Abaqus

5.1.1 Determination of the coordinates of the vertices of each element

In order to make use of equation 4.2, it is necessary to determine the coordinates of the center of the elements. However, Abaqus does not have a function that allows one to determine it directly.

Being so, the first step is to create a cycle 'for' which will go through all the elements and determine the connectivity of each element. The reason why connectivity has to be determined is because it is the only way to determine the coordinates of each vertex. As an example, the code used to determine the coordinates of one vertice is introduced in Appendix C.

5.1.2 Determination of the coordinates of the center of each element

Once determined the coordinates of the four vertices, it is possible to determine the coordinates of the center. It is not as straightforward given the fact that the elements are not always rectangles.

The code written in Pyhton (e.g. for only one of the center of the triangles, since it is similar for the other 3) is also in Appendix C.

In order to determine the centroide, one diagonal should be drawn and the center of each triangle (represented in yellow) is determined, as exemplified in figure 5.1.

The other diagonal is drawn and the centers of the two triangles (represented in green) are also determined (Figure 5.2).

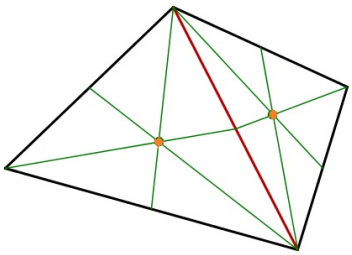

Figure 5.1: Step 1

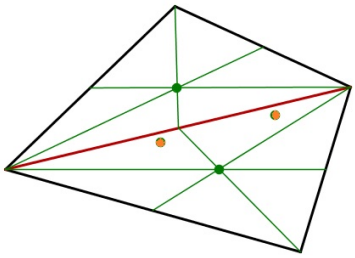

Figure 5.2: Step 2

Finally, the intersection point of the four points previously determined is the centroide of the quadrilateral.

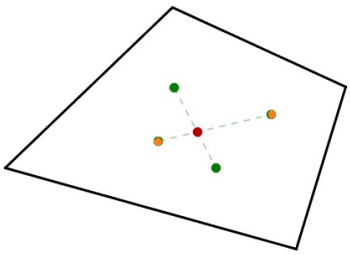

Figure 5.3: Step 3

Once the center is determined, it is finally possible to use equation 4.2, and determine the angle θ for each element.

From this point on is where the process diverges.

5.1.3 Definition of the material

As explained before there are two possible approaches.

The first approach makes use of the compliance matrix with a rotation angle equal to θ. Given this, the number of different materials defined is equal to the number of elements. In order to do so, the set of equations B.1 is implemented in the code and the entries of the compliance matrix are computed.

The second approach consists in creating a different composite layup for each element, where no further calculations are necessary once θ is computed.

Both approaches work, but a main difference between them was fundamental to choose one over the other: computational time. The second approach consumes way more time. However, it was very useful

to verify that the fibers are correctly placed, since it is the only process that allows the visualization of the placement of the fibers.

Given this, in the different scripts, the first approach is the one that prevails.

5.2 Introduction to the Printing Technology

Even though a prototype is not going to be manufactured, the algorithm of the path planning was built in order to meet the requirements of the printing process. As mentioned before, the printer used as reference is the Mark Two.

The printer provides two different fibre deposition strategies: isotropic and concentric [49]. The isotropic strategy consists in filling the selected area with parallel tows along a given orientation: the result is a sort of unidirectional ply. An example is presented in fig 5.4(a).

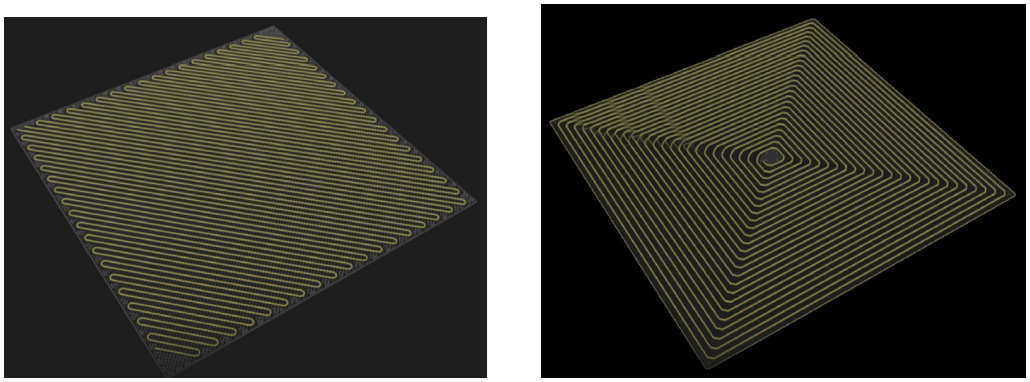

(a) Isotropic printing strategy [49]

(b) Concentric printing strategy [49]

Figure 5.4: Printing Strategies using Mark Two

Conversely, the concentric deposition option places the fibres by starting from the outer profile of the selected area and by filling the internal region by means of concentric paths: the result is a sort of spiral path, as illustrated in figure 5.4(b).

However, the technology allows placing the fibres in a single strand as long as possible to obtain a true VAT laminate with an unconventional fibre path [49].

Another appealing feature of Mark Two is that the printing process can be set in pause at a specific layer to add additional parts to the component, e.g., the user can introduce external parts like fasteners, in order to create a functional assembly.

5.3 Path Planning and Printing Time for straight Fibers

5.3.1 Path Planning

As mentioned before, one of the variables to be optimized was the printing time, and in order to do so, it was necessary to determine the path planning first.

The main goal when implementing the algorithm was to obtain a robust and continuous deposition path planning, and without causing under-deposition or over-disposition. Raster filling pattern has been developed since the need of providing directional properties to printed composites has began.

This algorithm was based in [74], and it was implemented in MATLAB.

5.3.1.1 Importing STL files

Before moving on and start describing the path planning itself, it is necessary to first explain how to obtain the geometry of the part.

The design of the part is done using a CAD software, and then imported as an ASCII STL file to MATLAB. The function is available at MATLAB'S File Exchange, and from the file it obtains the points and vertices of the original geometry. The function is considerably fast since it uses the *textscan* function instead of reading the file line by line.

5.3.1.2 Methodology

Important information regarding each layer is required before the definition of the deposition points. There are outer curves enclosing the inner contour curves, and the minimum and maximum points are determined along the scanning direction.

Raster fill methodology is used to generate a continuous deposition path along the scanning direction. The algorithm is implemented to obtain printing instructions for complex geometries.

5.3.1.3 Raster Filling Methodology

When printing a part, it is divided in several layers along the z direction, also known as the slicing process, and each layer is filled sequentially and independently. The slicing part was not explored since the study is mostly done in 2D.

The determination of the deposition path points are obtained by intersection of several lines along the y axis, within a distance of *D* between each line, with the outer contour. This distance is pre-defined, and in this case it will be considered 0.1mm (which is the layer resolution of the Markforged Mark Two Industrial Strength® 3D Printer). In order to reproduce the path planning in MATLAB, the equation used to plot the lines is:

$$y = tan(\alpha)x + b \tag{5.1}$$

where α is the angle of the fibers and b is the value of y when x=0. Since the spacing between lines has to be the same, it would be straightforward to increase b by that value if the lines were horizontal. However, when the angle starts to increase, one cannot simply add D to b and plot the line. The following scheme provides a better look of the problem, which is not complex, but it is an important detail:

From the scheme, D=0.1mm and α is the inclination of the line. Then, from basic trigonometry:

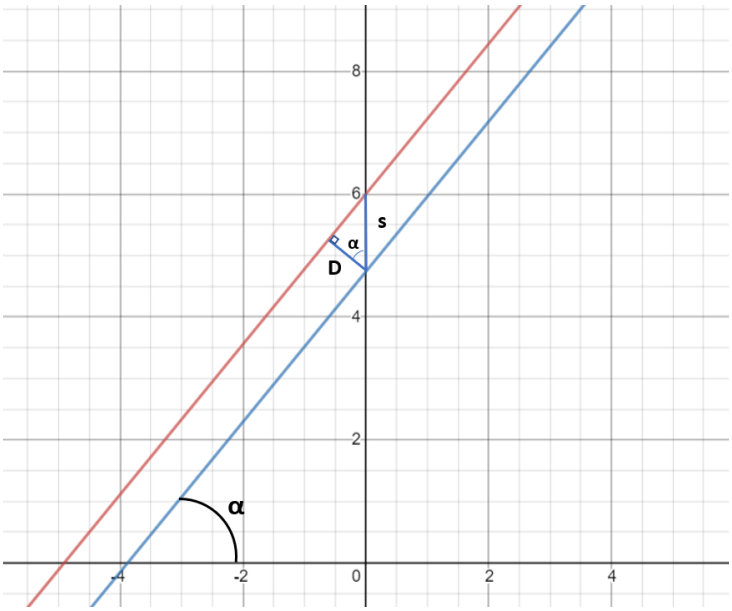

Figure 5.5: Spacing between lines

$$s = \frac{D}{cos(\alpha)} \tag{5.2}$$

Finally, s is then the value one has to add to the line equation in order to get the right spacing.

There are 2 cases that must be considered regarding only convex shapes: the existence or not of holes.

In the simpler case without holes, each horizontal line produces two intersection points. The lines are referred as either ”even” line or ”odd” line, being the first line ”even”, the second ”odd”, and so on. Regarding the intersection points, in the even line, it goes from ip_0 to ip_1, and in the odd line it goes the other way round, from ip_1 to ip_0 [74]. A scheme is introduced in figure 5.6, in order to clarify what was explained in this paragraph.

Figure 5.6: Raster Filling scheme

The part is created by filling from the layer with smallest z to the layer with the higher z. After filling one layer, the nozzle moves upwards, and the process carries on until the whole part is generated.

Considering the parts with holes, the process described until here cannot be applied since there is some information missing, such as the number of intersection points along each line.

5.3.1.4 Avoiding deposition outside the part

In concave shapes, or when there are holes in the part, when moving from an even line to an odd line, the deposition points can be far from each other in terms of x, meaning that there is a possibility of a deposition outside the boundaries of the part occurring (Figure 5.7).

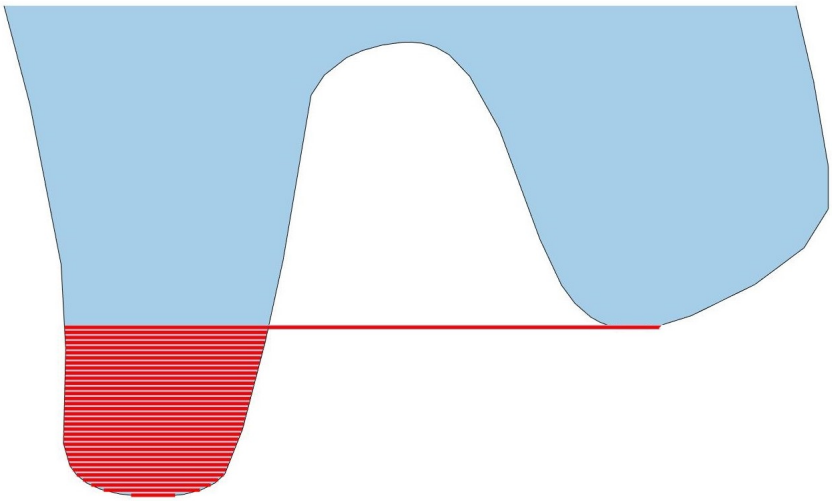

Figure 5.7: Deposition outside the part

So that one can prevent this for happening, whenever the horizontal lines are intercepting the boundaries of the part more than three times, then, it is possible to set that between the second and the third point, along each line, there cannot be deposition.

In order to check if this is happening or not, it is taken the curve between two consecutive lowest x points. If the y value is increasing, then there is no deposition outside the curve. If the y values are decreasing, then there is deposition.

Two examples of path planning are introduced in figures 5.8 and 5.9 for two different orientations, 0 and 30 degrees:

Once the path planning is explained, it is also important to describe the computation of the printing time, since besides the continuous path planning, the main goal was to optimize the printing time.

Previously in this work, it was mentioned that the Markforged Mark Two Industrial Strength® 3D Printer is the best in the market for CFRP composites and VAT composites, and it was used already in some researches and provided very good results [49].

However, not enough details of the printer are available, since for the model in which the study was based [75], it was mandatory to know the maximum and minimum velocities at which the printer could print and the acceleration. In [75], the printer used is not specified, however, since the path planning strategy was the same and also the technique (FDM), the values used were assumed accurate for this work.

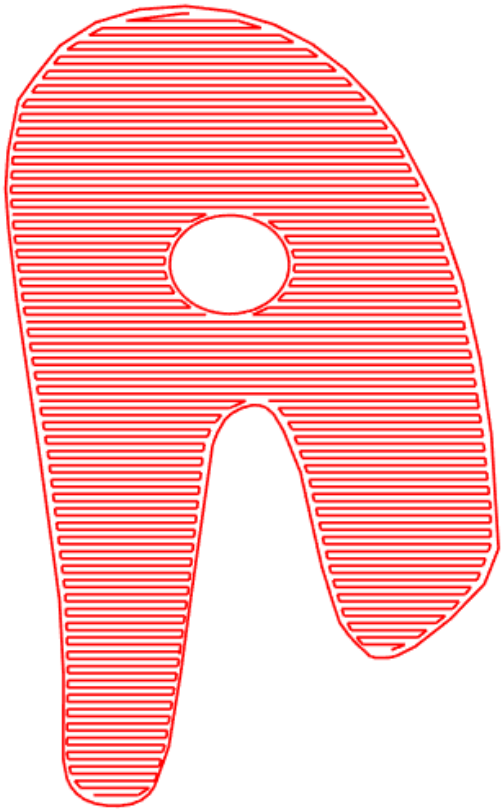

Figure 5.8: Path Planning for 0 degrees.

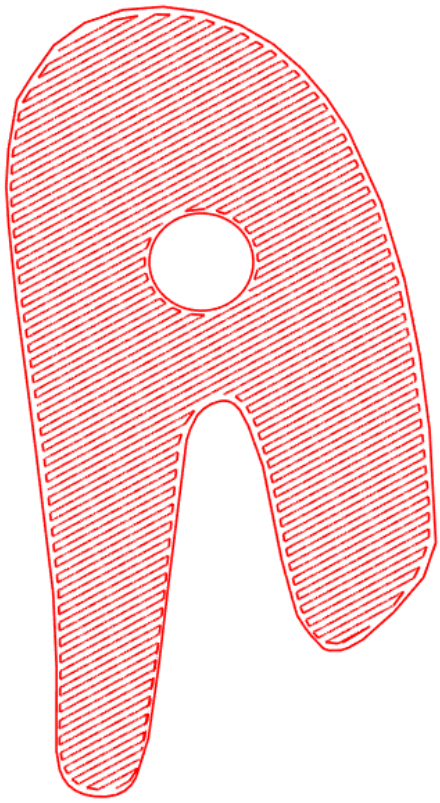

Figure 5.9: Path Planning for 30 degrees.

A further description of the method is explained next.

5.3.2 Printing Time

In zigzag path planning, it is possible to find two different types of lines *Type I* and *Type II*. The *Type I* zig zag lines form the main path whereas *Type II* zigzag lines are the connection lines between two *Type I* lines. An example is introduced next, in order to clarify the difference between the lines:

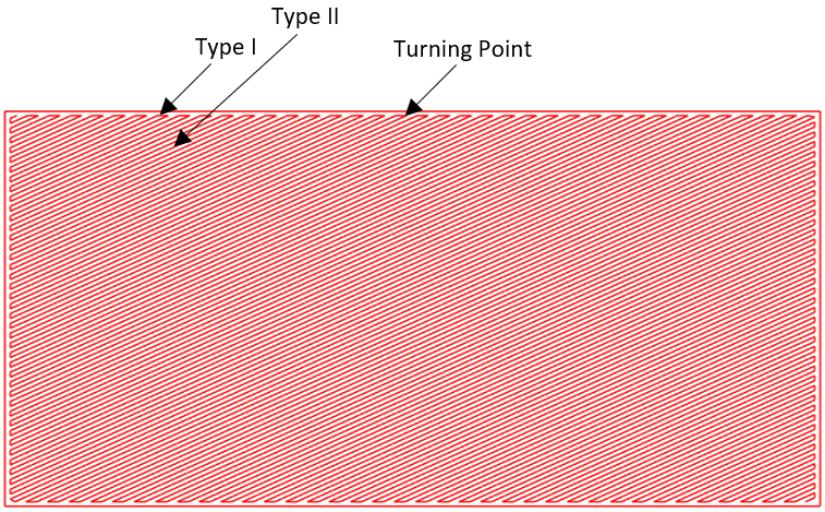

Figure 5.10: Types of zigzag lines

For both types of lines, the procedure when talking about the nozzle head is exactly the same: it starts with a minimum speed, afterwards it accelerates towards a maximum speed and then it decelerates to a minimum speed by the end it reaches the end of the line.

Having this said, the model aims to improve the efficiency of the process by accelerating or decelerating the nozzle according to the geometrical characteristics. As thus, the following assumptions are made:

- The speed of the nozzle as from all the turning points in the minimum speed, V_{min};
- The maximum speed is represented as V_{max}. Both velocities vary according to the printer's settings, however, in this model the assumption is that V_{max} equals twice V_{min};
- The velocity of the nozzle along the zigzag path is either uniformly accelerated or decelerated, and the acceleration is represented by β.

Following this assumptions, it is possible to rewrite it using equations:

$$V_{max} = 2 \times V_{min} \tag{5.3}$$

$$V_{max} = V_{min} + \beta t \tag{5.4}$$

where t represents the time needed in order to speed up the nozzle from V_{min} to V_{max}.

From equations 5.3 and 5.4, one can concludes that:

$$t = \frac{V_{min}}{\beta} \tag{5.5}$$

Also, the length L of each line can be computed using the following equation:

$$L = \frac{1}{2}\beta t^2 + V_{min}t \tag{5.6}$$

Combining equations 5.5 and 5.6, the following equation is obtained:

$$L = \frac{3V_{min}^2}{2\beta} \tag{5.7}$$

Based on the previous analysis, there are three different possible cases:

- If the length of the line is inferior to $\frac{3V_{min}^2}{2\beta}$, than the length is not big enough in order for the nozzle to reach V_{max}, as shown in Figure 5.11;
- If the length of the line is equal to $\frac{3V_{min}^2}{2\beta}$, than the V_{max} will be reached halfway through the line, as shown in Figure 5.12;
- If the length of the line is greater than $\frac{3V_{min}^2}{2\beta}$,than the V_{max} will be reached before the middle of the line, as shown in Figure 5.13.

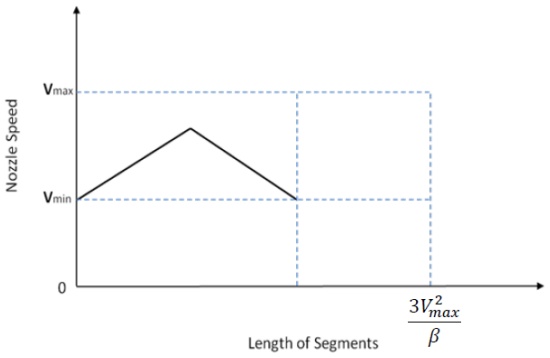

Figure 5.11: $L < \frac{3V_{min}^2}{2\beta}$ [75]

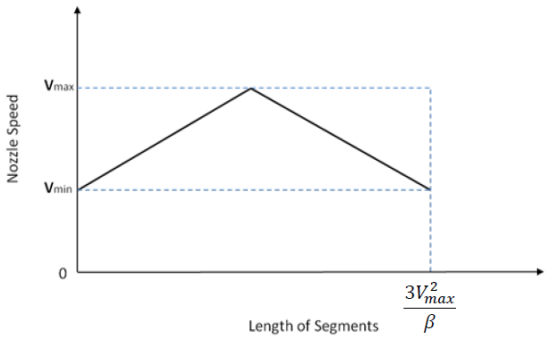

Figure 5.12: $L = \frac{3V_{min}^2}{2\beta}$ [75]

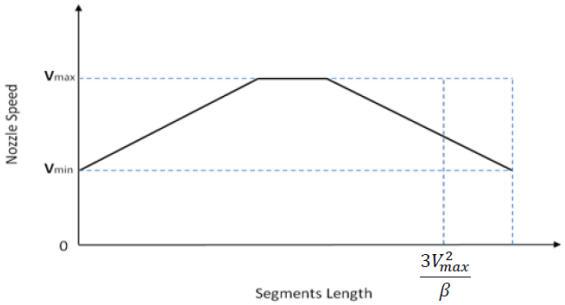

Figure 5.13: $L > \frac{3V_{min}^2}{2\beta}$ [75]

Finally, summarizing the formulas for each type of line:

$$Time(L_I) = \begin{cases} \frac{2V_{min}}{\beta}, & \text{if } L_I = \frac{3V_{min}^2}{\beta} \\ \frac{-2V_{min}}{\beta} + \sqrt{\left(\frac{2V_{min}}{\beta}\right)^2 + \frac{4L_I}{\beta}}, & \text{if } 0 < L_I < \frac{3V_{min}^2}{\beta} \\ \frac{2V_{min}}{\beta} + \frac{\beta L_I - 3V_{min}^2}{2\beta V_{min}}, & \text{if } L_I > \frac{3V_{min}^2}{\beta} \end{cases} \tag{5.8}$$

$$Time(L_{II}) = \begin{cases} \frac{2V_{min}}{\beta}, & \text{if } L_{II} = \frac{3V_{min}^2}{\beta} \\ \frac{-2V_{min}}{\beta} + \sqrt{\left(\frac{2V_{min}}{\beta}\right)^2 + \frac{4L_{II}}{\beta}}, & \text{if } 0 < L_{II} < \frac{3V_{min}^2}{\beta} \\ \frac{2V_{min}}{\beta} + \frac{\beta L_{II} - 3V_{min}^2}{2\beta V_{min}}, & \text{if } L_{II} > \frac{3V_{min}^2}{\beta} \end{cases} \tag{5.9}$$

5.4 Path Planning and Printing Time for Curved Fibers

The path planning algorithm with fixed angle is easy to both design and manufacture. Besides, it fulfills the requirement of strength and technology. However, it fails to explore the performance of the fiber to its fullest.

In this process, the variable angle path planning algorithm is that the fiber laying angle is always changing during the process. This angle is defined as the intersection angle between the direction of the

fibre laying and the x axis and which is always changing, as explained previously in subsection 4.2.2.

5.4.1 Path Planning

Regarding the path planning of the curved fibers, the algorithm is exactly the same. However, instead of straight lines, curved lines are ploted using equation 4.3. The same example used for straight fibers will also be introduced (Figure 5.14), this time with curved fibers. However, one detail should be emphasized: For this case, the first curved was drawn, and then the others are designed using the shifted method. This is particular important for the case studies that will be introduced further in this thesis, and also for the definition of the angle ϕ.

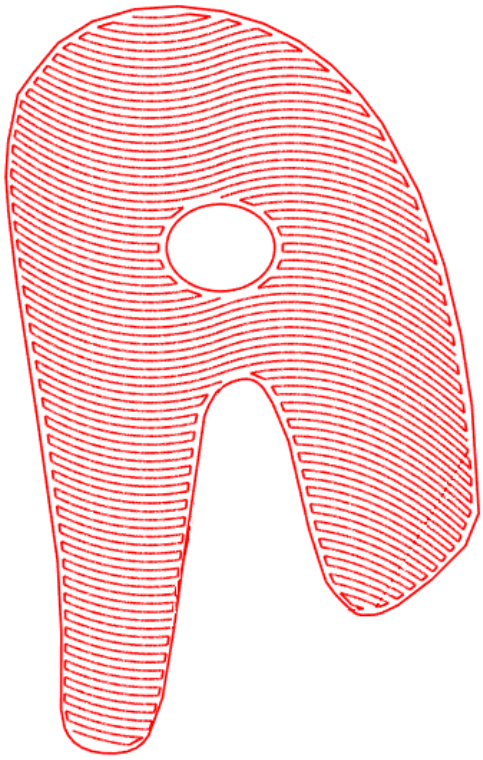

Figure 5.14: Path Planning for $T_0 = 0.45$, $T_1 = -0.35$ and $\phi = 0$.

5.4.2 Printing Time

Even though the previous equations were only applied to 3D printing of straight fibers, they were also used for curved fibers. The printing velocity and the acceleration were assumed to be the same. Further in this work, when the case studies are introduced, the values of both velocity and acceleration will be given.

Besides this, what has changed when compared to straight fibers is the determination of the length of each curve, giving the fact that it is not as straightforward.

The formula implemented was the one that determines the length of a curve y=f(x) that goes from x=a to x=b:

$$L = \int_a^b \sqrt{1 + \left(\frac{dx}{dy}\right)^2} \tag{5.10}$$

5.5 Optimization

Most of the objective functions are formulated based on energy form, and strain energy formulation is one of the general formulation for optimization methods.

The objective function in this method aims to minimize the sum of all the element's strain energy. Using this concept of element strain energy, the deformations in all the directions are considered. Also, since strain energy and stiffness are inversely proportional, it means that a lower value of strain energy leads to a higher stiffness.

Before moving on to explaining both types of optimizations used, it is important to explain a change made in the code in order to prevent losing the results up until the point where it was in case that a crash happens. Since there are several population generations per iteration, and also several iterations, and because there is a link between MATLAB and Abaqus, it happened, especially in the case of curved fibers, since it is more demanding when it comes to the FEA, the optimization stopped and the only option was to restart. The solution found for this case was to use the last population as initial population in the next optimization. Important to refer than whenever there is no crash, the first population is generated randomly. Obviously, the number of generations left to end the optimization have to be updated.

The partial code which allows to restart the optimization from the stopping point in case of a crash is introduced in Appendix C.

5.5.1 Strain Energy Based Optimization Method

Considering a force applied on a body, this force is directly proportional to the deflection within the elastic limit, according to Hook's Law. The area under the force vs deflection curve is the work done in order to produce the deflection. This work is stored in the structure as strain energy. The mathematical formulation is the following:

$$U = \frac{1}{2} \int_T \{\sigma\}^T \{\epsilon\} \, dV \tag{5.11}$$

where U is the strain energy, σ the stress vector, ϵ is the strain vectors and V is the total volume of the body.

Considering a 2D element on which different normal and shear stresses, σ_{xx}, σ_{yy}, τ_{xy} and τ_{yx} are acting, the strain energy of this element is given by:

$$U = \frac{1}{2} \{\sigma_{xx}\epsilon_{xx} + \sigma_{yy}\epsilon_{yy} + \tau_{xy}\gamma_{xy}\} \, dV \tag{5.12}$$

When it comes to stiffness, it is defined as the resistance of an elastic body to deformation by an applied force. As it was already mentioned, stiffness and strain energy are inversely proportional to each

other, meaning that if the body has less strain energy values, then it will be stiffer.

Having this said, the element strain energy values will be used as objective function in the optimization proposed in this paper.

The optimization problem is defined as [76]: finding the trade off between the best angle for the fibers, so that the stiffness of the work piece is maximized, and the minimum printing time. This stiffness is achieved in terms of strain energy of the work piece. The formulation of the optimization problem is:

$$\text{Minimize:} \qquad F = w_u \sum_{i=1}^{n} u_i + w_{time} \sum_{i=1}^{n} time_i \qquad i = 1, 2, 3, ..., n \tag{5.13}$$

$$\text{Subject:} \qquad -90 < \alpha_i < 90 \qquad i = 1, 2, 3, ..., n \tag{5.14}$$

where,

F: Objective function;

w_u: weight associated with the sum of the strain energy;

u: Strain Energy of Finite Elements;

w_{time}: weight associated with the printing time;

$time$: Printing time of the part;

n: Number of Elements.

As mentioned before in this thesis, the optimization problem is solved using the genetic algorithm, which is one of the most efficient optimization algorithms.

5.5.2 Stress Based Optimization Method

The most common optimizations are usually focused on the global structural behaviour, such as stiffness and frequencies. However, when aiming for a real optimum design of a structure, stresses must be considered, and doing so, there are two major difficulties that have to be faced:

- Increased computational complexity, since a larger number of variables have to be considered, given that unlike stiffness, stress is a local quantity;
- Stress is highly non-linear with respect to design variables, resulting in a special given to the move limit, in order to achieve convergence.

In this work, the solution introduced to solve the local stress problem is to transform the stresses into a global stress measure. Being so, this global stress measure will be the only constraint considered in the process.

There are two clear advantages:

- It makes the algorithm easier;
- It reduces the computational cost for calculating the elemental stress sensitivities.

The major drawback is the difficulty in finding a general and robust function. In this work, the function that is used is Kreisselmeier-Steinhauser (KS) [77]:

$$G_{ks} = \frac{1}{p} \ln \sum_{i=1}^{N} e^{p \frac{f_i(\sigma)}{f_{max}(\sigma)}} \tag{5.15}$$

where,

G: Objective function;

σ: Stress;

$f_{max}(\sigma)$: Maximum von Mises stress;

$f_i(\sigma)$: von Mises stress for each finite element;

$time$: Printing time of the part;

n: Number of Elements.

For this thesis in particular, it is also important to consider the printing time, as mentioned before, and being so, the ultimate objective function which have to be minimized is written as follows:

$$F = w_\sigma \frac{1}{p} \ln \sum_{i=1}^{N} e^{p \frac{f_i(\sigma)}{f_{max}(\sigma)}} + w_{time} \sum_{i=1}^{n} time_i \tag{5.16}$$

where,

F: Objective function;

w_σ: weight associated with the stress;

w_{time}: weight associated with the printing time;

The parameter p sets the difference between the original function and its approximation. A higher p means a more heavily weighted peak stress. However, it often leads to oscillation and divergence. The p considered is p=20 [77] and its selection is beyond the scope of this thesis.

5.6 Mesh Convergence

Even though it is not mandatory, a sufficiently refined mesh will assure that the results from the FEA are adequate, since the refinement influences the accuracy and convergence of the results. A mesh is said to converge when further refinement produces residual changes in the solution. This would give us confidence that for the given model, the simulations will reproduce mathematically accurate and reliable solutions every time [78].

The mesh convergence study can be performed by monitoring any parameter in the system. Having this, the total strain energy will be the chosen parameter.

Since there are different geometries to be studied, and within those geometries, two different types of fibers, four different convergence studies were performed. However, the results are supposed to be the same for the same geometry, regardless the type of fibers. The geometries are:

- Plate without hole;
- Plate with hole;

  The several simulations showed that the strain energy converges at minimum element sizes, which will be listed after the plots, and further decrease of this size would only result in higher computational time, which is unnecessary.

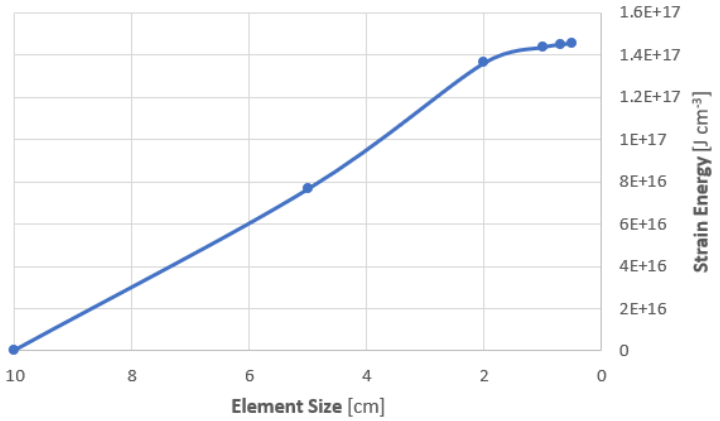

(a) Straight Fibers - 0.5 cm

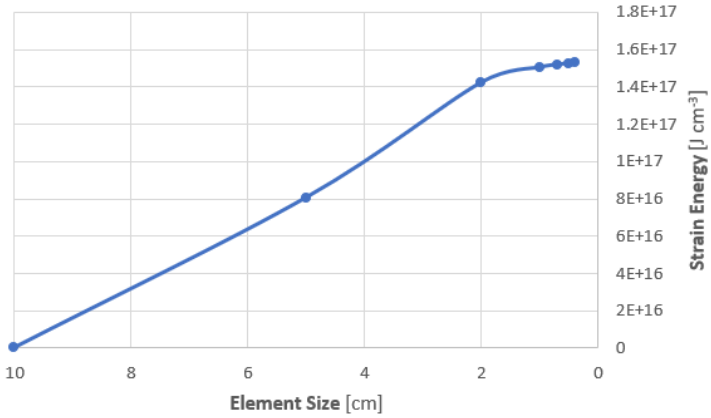

(b) Curved - 0.5 cm

Figure 5.15: Mesh Convergence for both straight and curved fibers in a fully clamped shell plate under constant pressure

Regarding the plots, for both geometries, the element size at which the convergence is verified is 0.5 cm.

Being so, the main goal of this study was to determine the maximum element size at which convergence exists, since simulations with the genetic algorithm are already extremely heavy computational wise.

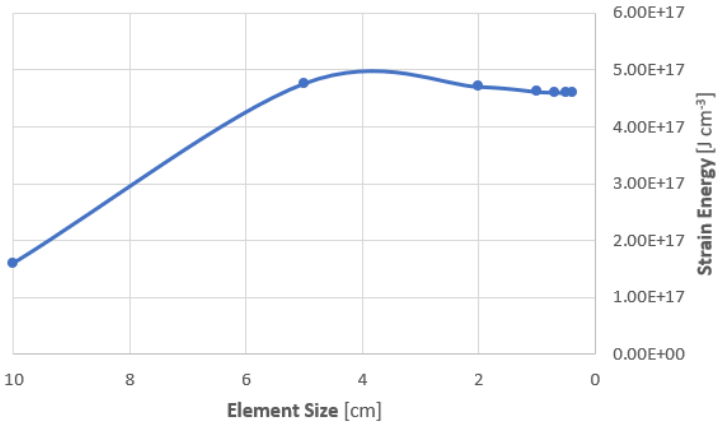

(a) Straight - 0.5 cm

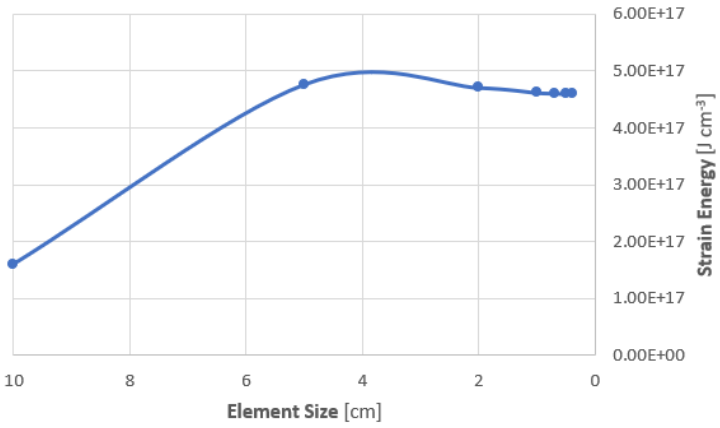

(b) Curved - 0.5 cm

Figure 5.16: Mesh Convergence for both straight and curved fibers in fully clamped shell plate under constant pressure with a hole in the middle

Chapter 6

Results

In this chapter, both case studies and results will be discussed and introduced. Regarding the case studies, geometry, boundary conditions and applied loads will be specified for each one. It is important to mention that the case studies are the same for both straight and curved fibers.

Once the case studies are introduced, the results obtained from the performed optimization will be presented, analyzed and discussed. The final part of the chapter is divided in three main sections: Shell plate without a hole; Shell Plate with Hole and 3D Specimen. In each of these sections, different optimized solution are presented for straight and curved fibers. It is also important to highlight that, in order to obtain good and explicit figures, when plotting the path planning the diameter was considered 4 mm instead of 0.1 mm. The other computations were all performed with the value of 0.1 mm.

6.1 Case Studies

The geometry of each case will be introduced at the same time the cases are described. The geometry, boundary conditions and applied loads are the same for both straight and curved fibers.

However, before going further in detail in each one, considering the mechanical behaviour, further details have to be added to clearly define the theoretical framework of this work:

- The geometry of the laminate and the applied BCs are known and fixed;
- Each case, besides the 3D one, only considers one ply;
- The material behaviour is linear elastic;
- The VAT plate is quasi-homogeneous and fully orthotropic [79] [80] at each point of the structure.
- The speeds are assumed to be the same for both straight and curved fibers: $V_{max} = 20mm/s$, $V_{min} = 10mm/s$ and $\beta = 20mm/s^2$.

– All the results were scaled in order to perform the optimization, so that the values would be of the same order of magnitude. The results shown below are not scaled.

After stating the overall process to determine the optimized design, and once explained in detail each step, the different cases will be now introduced. First the 2D cases will be described, and finally the 3D case. Once again, it is also important to highlight that each 2D case will be simulated for both strain and stress optimization.

6.2 2D Cases

6.2.1 Shell Plate without a hole

The first case to be presented is a shell plate without a hole. The reason why this case is introduced is in order to validate the optimization process. Even though the values will not be directly compared, it is important to evaluate if the results are consistent with the theory. Having this, and especially to this end, this geometry will be studied under two different loads. It is extremely hard to compare the following case studies of straight fibers with possible analytical solutions, and it becomes even more demanding given the fact that the fabrication process of these parts is different from the traditional manufacturing processes. Moreover, the curved fibers are even more difficult to verify, since there is not an existent model defined for curved fibers, to the best knowledge of the author.

The dimensions of the part are 260mm x 160mm. The finite element model of the plate is shown in Fig. 4. The elements in use are S4R. O (0, 0, 0) is the origin point.

Two different sets of boundary conditions and loads are going to be considered:

– Fully clamped plate in bending, where distributed pressure of magnitude 10000 Pa is applied in the - Z-direction. (Figure 6.1a));
– Plate under traction, with the left side clamped (x=-13) and a force of magnitude 10000 N applied in the X-direction, on the right side of the plate (x=13) [6.1b)].

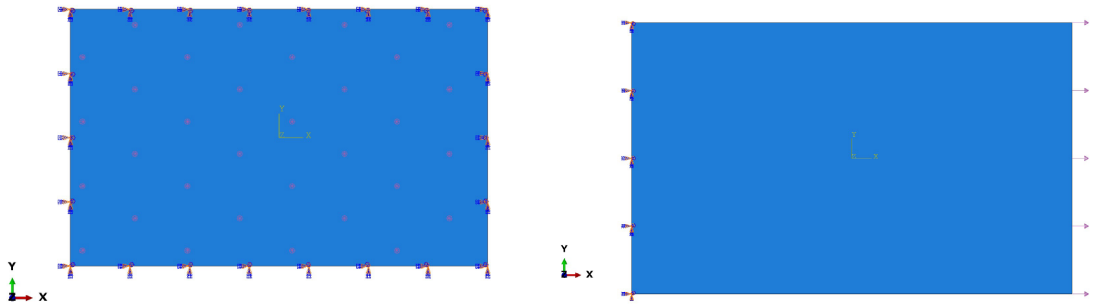

(a) Fully Clamped Plate under Uniform Pressure (b) Plate under traction

Figure 6.1: Plate without a hole

6.2.2 Shell Plate with a Hole

This case is similar to the previous one when it comes to boundary conditions and regarding the load, the traction case will not be applied. However, the geometry is slightly different, since there is now a hole in the center of the plate. This will result in a accumulation of stress around it, leading to more interesting results. Similarly, a figure is introduced to clarify the case scenario:

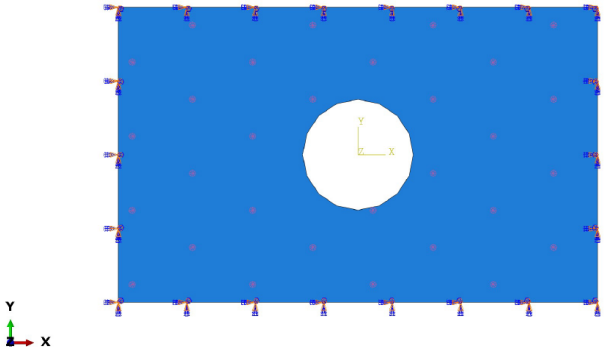

Figure 6.2: Fully Clamped Plate under uniform pressure

It is also important to clarify, for the case of the curved fibers, how will they be defined in these cases. Basically, the angle T_0 is defined in x=0, and the angle T_1 is defined in x=-13 and x=13, meaning that the length d is dependent on the angle phi, and finally, ϕ=0 it is aligned with the x axis. Furthermore, and as mentioned before, the curves following the first curve will be defined using a shifted method. Given this, and with the main goal of being able to define the curve along the whole length of the rectangle, then the angle ϕ will only vary between $-tg^{-1}(8/13)$ and $tg^{-1}(8/13)$. The author is aware of the fact that this constraint will limit the results obtained, but the ones obtained will be significantly more accurate.

6.2.3 3D Specimen

The main goal of this work was to investigate and conclude the best design for each case, once optimized, in two dimensions. However, a 3D case was also analyzed, since it is the most realistic. The case consists in a tensile specimen, with a hole in the middle, as represented in figure 6.3. The geometry was provided by the Sabanci University, Turkey.

The dimensions of the part are 38mm x 250mm x 1.016 mm, and it is composed by 8 layers, which means that each layers presents a thickness of 127E-03 mm. The mesh elements used are C3D8R. O (0, 0, 0) is the origin point.

Finally, regarding the boundary conditions, the specimen will be under traction, meaning that the right end of the specimen (y=-0.125) is fully clamped while the other end (y=0.125) is where the force (F=1000N) is applied.

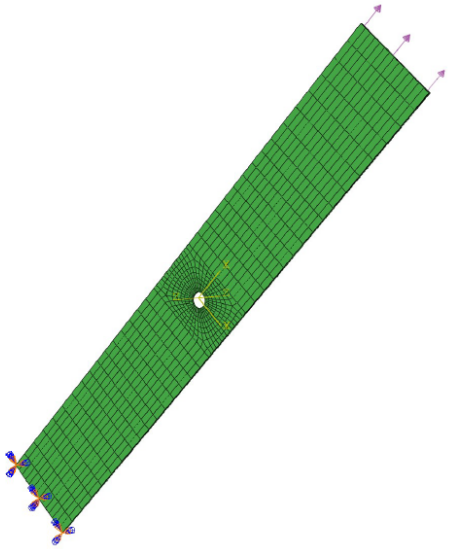

Figure 6.3: Tensile Specimen in Traction

6.3 Shell Plate without a hole

For Fiber-Reinforced Composites, when the fibres are aligned with the load they provide maximum strength, even though this strength is only along the direction of alignment. However, these results are valid and obtained when considering the weight of the strain (or stress) function as 1, the scenario may or may not change when the function of the path planning time is considered.

6.3.1 Strain Optimization

6.3.1.1 Straight Fibers

The optimization was performed for a set of different weights, and the results are summed up and gathered in table 6.1.

Table 6.1: Optimal solutions for the plate without hole and straight fibers - Strain Optimization

Weight_Time	Weight_StrainEnergy	Theta (degrees)	Printing Time (s)	Strain Energy (J)
1	0	0	21270	5.69e+15
0.5	0.5	90	21520	1.45e+15
0	1	90	21520	1.45e+15

Analyzing the table, the results for when both weights were set to 0.5 and when the strain was given the weight of 1 are the same, fibers oriented to 90 degrees. When only the printing time was taken into account (i.e. $w_{time} = 1$), the best orientation is 0 degrees, which makes sense, since the fibers are longer, and it gives time for the nozzle head to accelerate, furthermore, there are less turns, which leads to a higher speed in general.

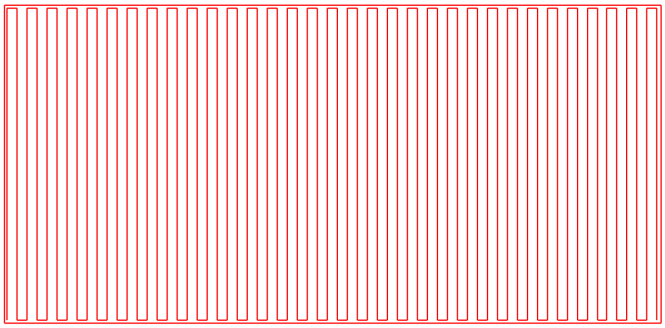

Figure 6.4: Strain Optimization for Straight fibers - Optimal Solution for the plate without a hole: $w_{time} = 0.5$ and $w_{strain} = 0.5$ & $w_{strain} = 1$ and $w_{time} = 0$

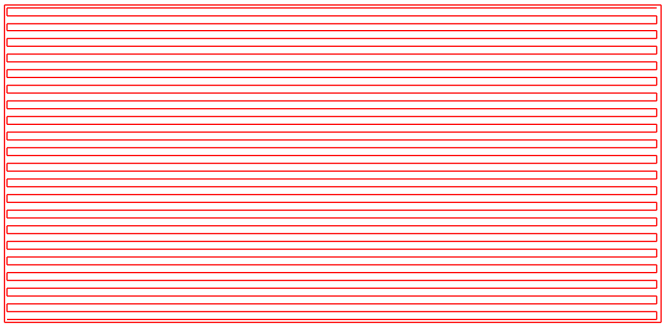

Figure 6.5: Strain Optimization for Straight fibers - Optimal Solution for the plate without a hole: $w_{strain} = 0$ and $w_{time} = 1$

When it comes to the case study where the shell plate is under traction, the optimization was only performed for when the weight factor of strain energy is 1. The results from the optimization and the plot of the optimal solution are introduced in table 6.2, below:

Table 6.2: Optimal solutions for the plate without hole and straight fibers, under traction - Strain Optimization

Weight_Time	Weight_StrainEnergy	Theta (degrees)	Printing Time (s)
0	1	0	21270

When the case study was first described, its objective was clarified as being a validation of the optimization process. According to the theory, for straight fibers, the best mechanical properties can generally be obtained for composites where the fibre is aligned parallel to the direction of the applied load [82], which means that for the case of traction introduced before (figure 6.6), the best fiber orientation would be 0 degrees. Finally, the case with a fully clamped shell plate with an applied pressure, it is expected that fiber orientation that provides the best stiffness for the part is

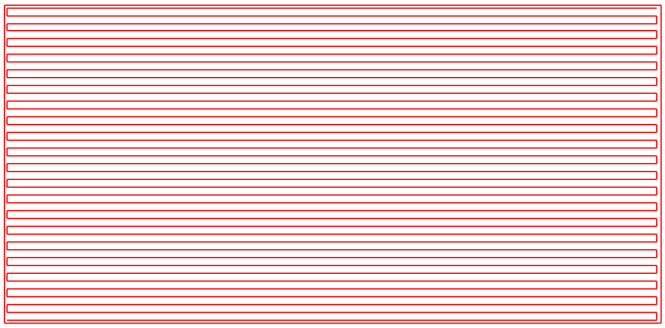

Figure 6.6: Strain Optimization for Straight fibers - Optimal Solution for the plate without a hole under traction: $w_{time} = 0$ and $w_{strain} = 1$.

the one that results in the shortest fibers. In this particular case, the minimum length of the fibers is accomplished when they are placed forming a 90 degrees angle with the horizontal axis, which means that the result obtain is coherent.

Once the straight fibers are validated, it is now time to validate the optimization of the curved fibers. Next, the results of the curved fibers will also be presented and analyzed, and a bridge is defined between them and the straight fibers.

6.3.1.2 Curved Fibers

Similar to the process followed for the straight fibers, also for the curved fibers the optimization was performed for 3 different set of weights, and a table with the different results will be presented. Contrary to table in the previous section, this new table will have three different angles:

Table 6.3: Optimal solutions for the plate for different weight combinations

Weight_Time	Weight_StrainEnergy	T_0 (degrees)	T_1 (degrees)	Phi (degrees)
1	0	2.32	6.23	-4.53
0.5	0.5	70.6	23.5	25.7
0	1	-59.6	-51.8	-23.1

Table 6.4: Optimal solutions for the plate for different weight combinations

Weight_Time	Weight_StrainEnergy	Printing time (s)	Strain Energy (J)
1	0	22246	6.64e+15
0.5	0.5	47878	6.31e+15
0	1	43094	5.47e+15

Considering the equation used to implement the curved fibers (section 4.2.2), it is easy to understand that for some angle combinations straight fibers are obtained. In this case, even with the weight variations, the designs which minimize the objective function are all straight fibers.

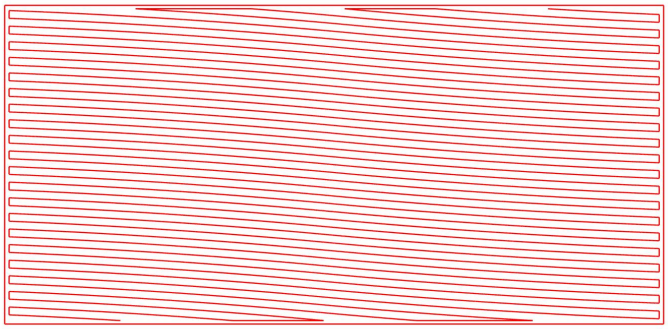

Figure 6.7: Strain Optimization for Straight fibers - Optimal Solution for the plate without a hole: $w_{strain} = 0$ and $w_{time} = 1$

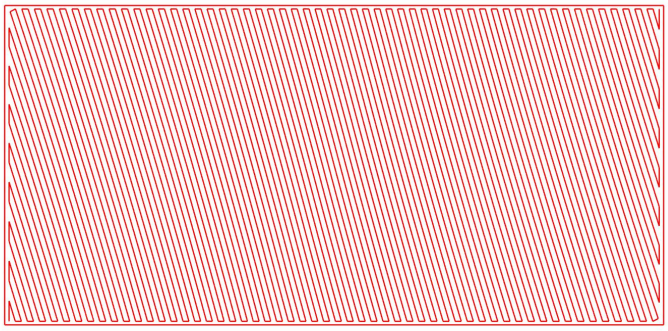

Figure 6.8: Strain Optimization for curved fibers - Optimal Solution for the plate without a hole: $w_{time} = 0.5$ and $w_{strain} = 0.5$

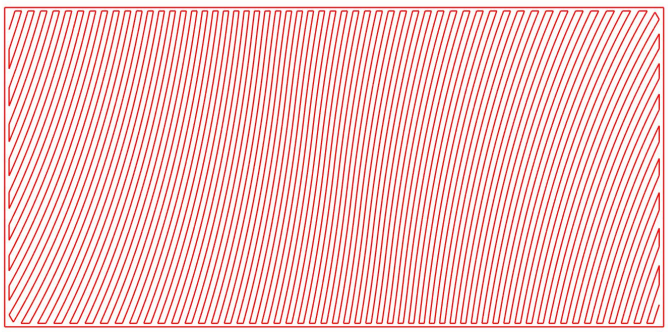

Figure 6.9: Strain Optimization for curved fibers - Optimal Solution for the plate without a hole: $w_{time} = 0$ and $w_{strain} = 1$

Analyzing the optimal solutions, it is possible to verify that the curved fibers degenerate in quasi straight fibers for this case. When the $w_{time} = 1$, the orientation tends to 0, as for straight fibers, and regarding the other two cases, even though the fibers are not exactly aligned with the vertical, it is possible to verify a tendency to be so.

The slightly difference that exists would probably fade if a higher limit was set for the Maximum Generation, when running the GA. Furthermore, the limitations imposed to the ϕ angle can also contribute to the existent differences.

In conclusion, considering the convergence study done in section 5.6 and the analysis of this case study for different loads, it is possible to validate the optimization process, for both types of fibers, and the limitation of not having analytical solutions to compare with was somehow overcome.

6.3.2 Stress Optimization

6.3.2.1 Straight Fibers

Similar to the structure of the previous sections, a table will also be introduced for the stress optimization in order to gather the results:

Table 6.5: Optimal solutions for the plate for different weight combinations - Stress Optimization

Weight_Time	Weight_Stress	Theta	Printing Time (s)	Stress
1	0	0	21270	1.137
0.5	0.5	-90	21520	1.212
0	1	27.6	21528	1.129

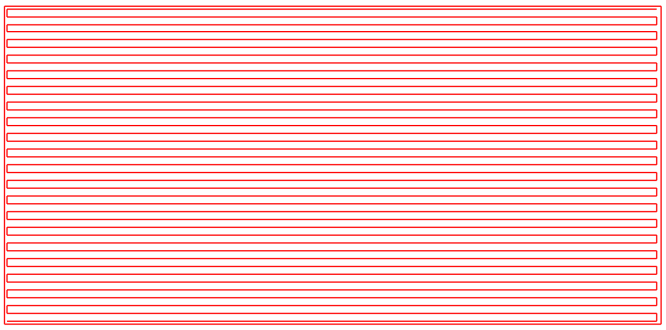

Figure 6.10: Stress Optimization for Straight fibers - Optimal Solution for the plate without a hole: $w_{time} = 1$ and $w_{stress} = 0$

For stress optimization, it is possible to observe that for when only the time is considered, the result is consistent.

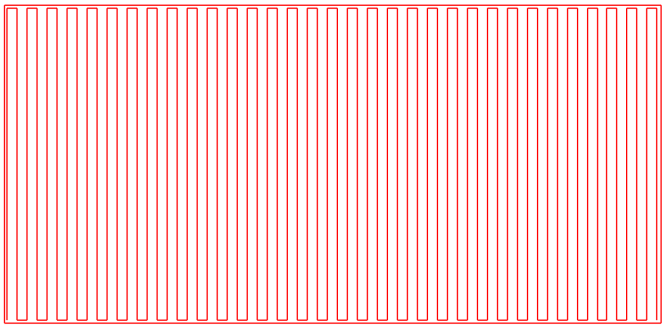

Figure 6.11: Stress Optimization for Straight fibers - Optimal Solution for the plate without a hole: $w_{time} = 0.5$ and $w_{stress} = 0.5$

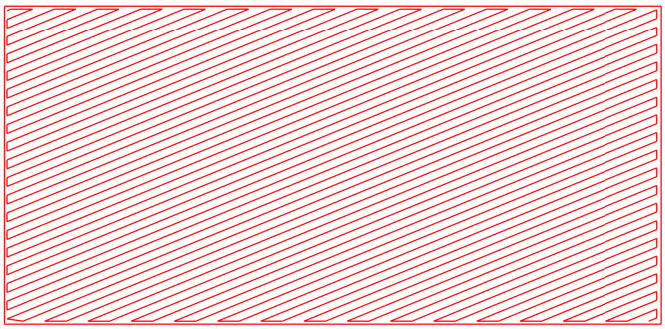

Figure 6.12: Stress Optimization for Straight fibers - Optimal Solution for the plate without a hole: $w_{time} = 0$ and $w_{stress} = 1$

Table 6.6: Optimal solutions for the plate for different weight combinations - Stress Optimization

Weight_Time	Weight_Stress	T_0 (degrees)	T_1 (degrees)	Phi (degrees)
1	0	2.26	6.15	-4.53
0.5	0.5	-59.3	-52.3	-16.9
0	1	22.5	63.7	0.226

Table 6.7: Optimal solutions for the plate for different weight combinations

Weight_Time	Weight_Stress	Printing time (s)	Stress
1	0	22242	1.111
0.5	0.5	36688	1.138
0	1	47063	1.104

6.3.2.2 Curved Fibers

Starting the analysis for the case when only the printing time is taken into account, the optimum solution is the same as the one presented in figure 6.9, which shows the coherence in the results. Regarding the other results, it is possible to observe that also the solutions tend to the orientations

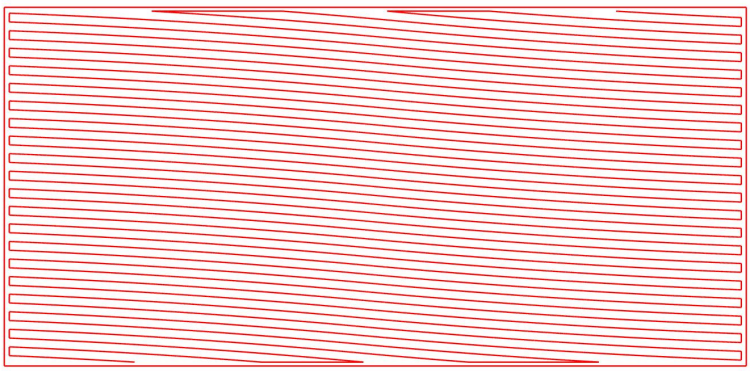

Figure 6.13: Stress Optimization for Curved fibers - Optimal Solution for the plate without a hole: $w_{time} = 1$ and $w_{stress} = 0$

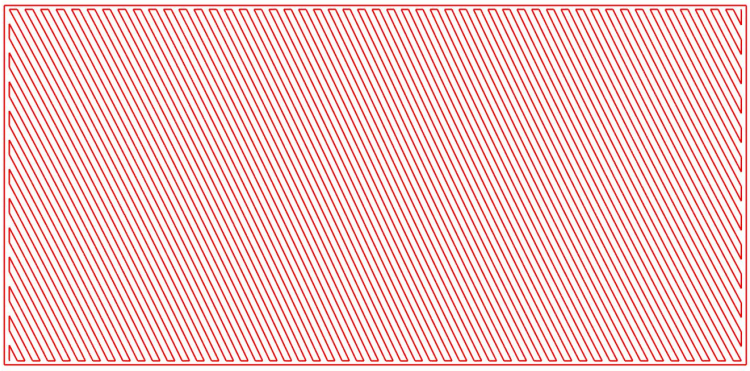

Figure 6.14: Stress Optimization for Curved fibers - Optimal Solution for the plate without a hole: $w_{time} = 0.5$ and $w_{stress} = 0.5$

computed using straight fibers. As expected, also given the complexity of the design process, the computing time is higher for curved fibers, however, the stresses values presented are lower.

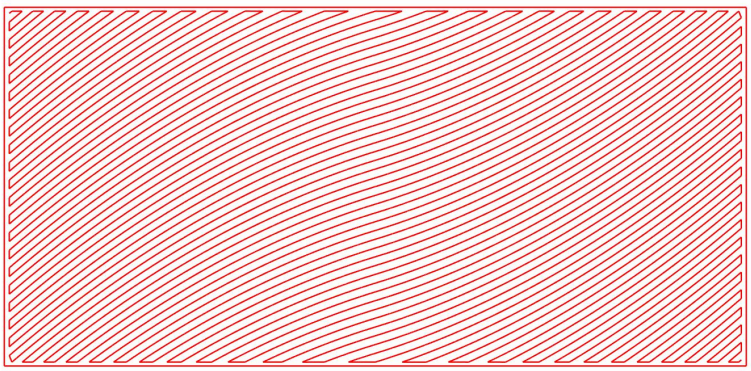

Figure 6.15: Stress Optimization for Curved fibers - Optimal Solution for the plate without a hole: $w_{time} = 0$ and $w_{stress} = 1$

6.3.3 Parametric Study for Straight Fibers - Shell Plate without a hole

As a complement for the validation done before, two parametric studies were performed: plate without a hole and Plate with a Hole.

Even though the optimizer uses Abaqus, and this result may seem redundant, it is not. And the explanation is simple, since the optimizer is always generating new populations, it could happen that the space of the design variables was not being explored to its fullest.

For the different orientations of straight fibers, a structural analysis in Abaqus was run, in order to validate the results for when the weight factor of the stress (or strain) is 1.

Two different optimizations were performed, and according to that, for the different simulations, both the strain and the stress Von Mises were extracted, in order to confirm the results. The final strain is equal to the sum of the strain energy of each element, and the final stress is computed using equation 5.15.

The plots with the results are introduced below:

For the first plot, and as expected, the minimum strain energy occurs for 90 degrees, which is the result obtained through the optimization process. When it comes to the stress, the minimum is obtained exactly for 27.6 degrees, which is the same result as the one obtained in the optimization.

6.4 Shell Plate with Hole

After the validation of the model with a simple case, the next results will be assumed correct and valid. As mentioned before, the fact that this geometry includes a hole will lead to more interesting results, given that it contributes to the accumulation of tensions.

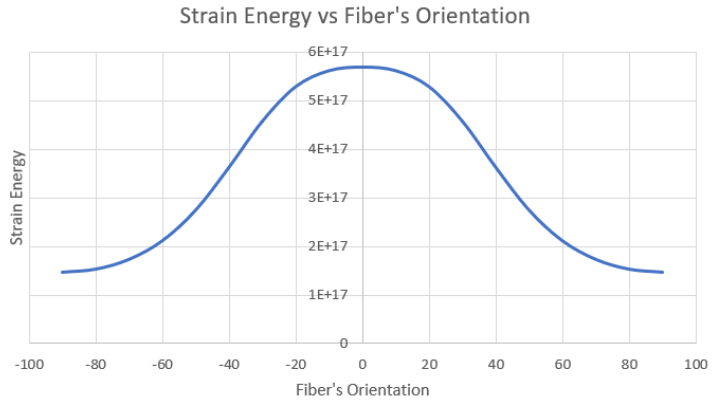

Figure 6.16: Parametric Study - Strain Energy

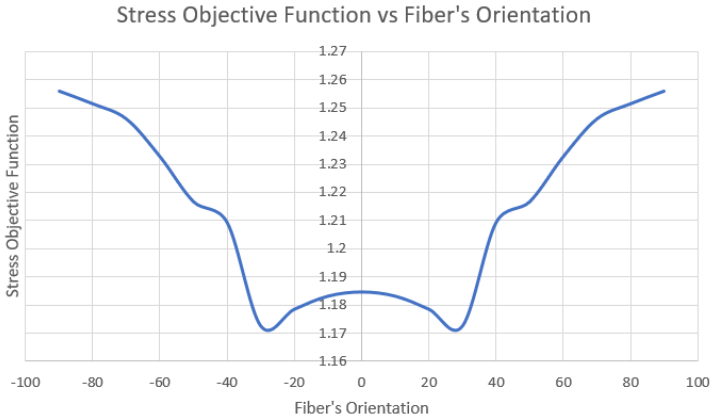

Figure 6.17: Parametric Study - Stress

6.4.1 Strain Optimization

6.4.1.1 Straight Fibers

Following the same plan, the weights for which the optimizations were run are the same.

Once again, a table summing up the results is introduced:

Table 6.8: Optimal solutions for the plate with a hole for different weight combinations - Strain Optimization

Weight_Time	Weight_StrainEnergy	Theta (degrees)	Printing Time (s)	Stain Energy (J)
1	0	0	20095	4.606e+15
0.5	0.5	-90	20277	1.197e+15
0	1	-90	20277	1.197e+15

When both weights are set at 0.5, and when only strain energy is taken into account ($w_{strain} = 1$), the best orientation is 90 degrees, as represented in the following figure.

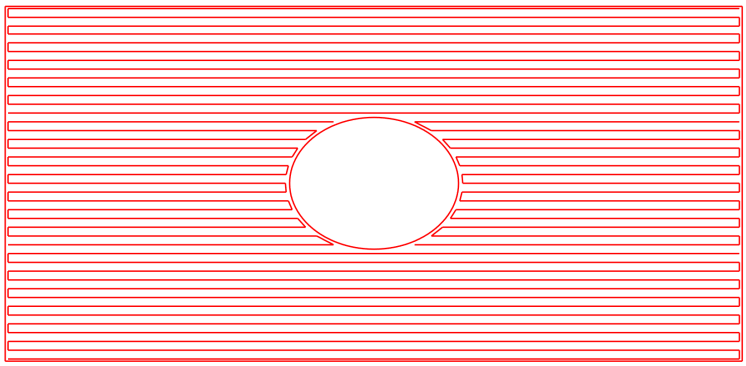

Figure 6.18: Strain Optimization for Straight fibers - Optimal Solution for the plate with hole: $w_{time} = 1$ and $w_{strain} = 0$

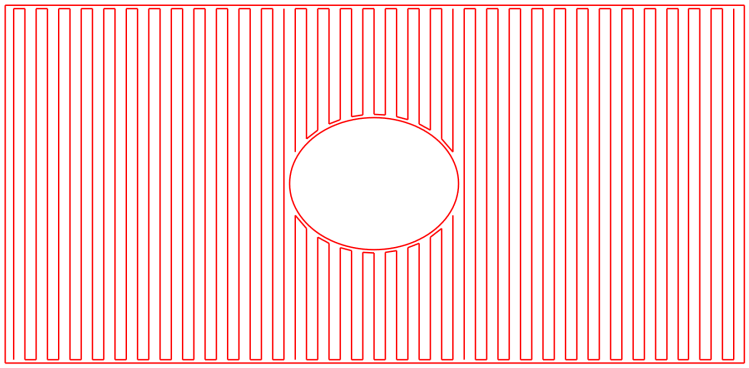

Figure 6.19: Strain Optimization for Straight fibers - Optimal Solution for the plate with hole: $w_{time} = 0.5$ and $w_{strain} = 0.5$ & $w_{strain} = 1$ and $w_{time} = 0$

6.4.1.2 Curved Fibers

Table 6.9: Optimal solutions for the plate with a hole for different weight combinations - Strain Optimization

Weight_Time	Weight_StrainEnergy	T_0 (degrees)	T_1 (degrees)	Phi (degrees)
1	0	1.69	5.52	-3.79
0.5	0.5	-82.7	-67.1	-23.5
0	1	-68.4	-68.4	-29.8

Once again, it is possible to see the curved fibers degenerate in straight fibers. Even though there is a hole and the curved fibers have the ability to adapt to it, since the optimization was strain energy based, these results were expected. As explained before, the hole will result in accumulated stresses around it, so it is expected to have more interesting results, i.e., that would further explore

Table 6.10: Optimal solutions for the plate for different weight combinations

Weight_Time	Weight_StrainEnergy	Printing time (s)	Strain Energy (J)
1	0	20983	4.64e+15
0.5	0.5	42752	2.05e+15
0	1	43831	1.78e+15

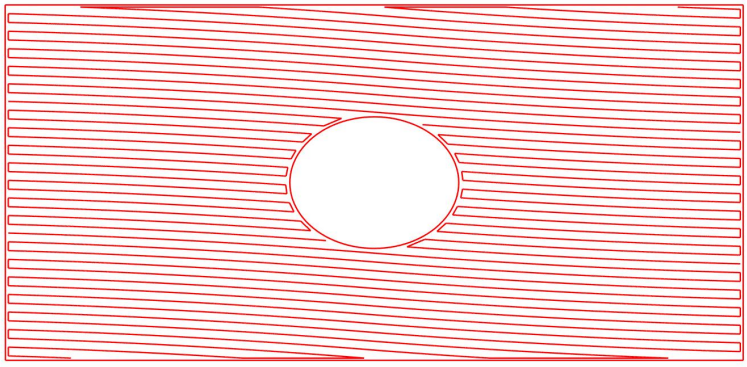

Figure 6.20: Strain Optimization for Curved fibers - Optimal Solution for the plate with hole: $w_{time} = 1$ and $w_{strain} = 0$.

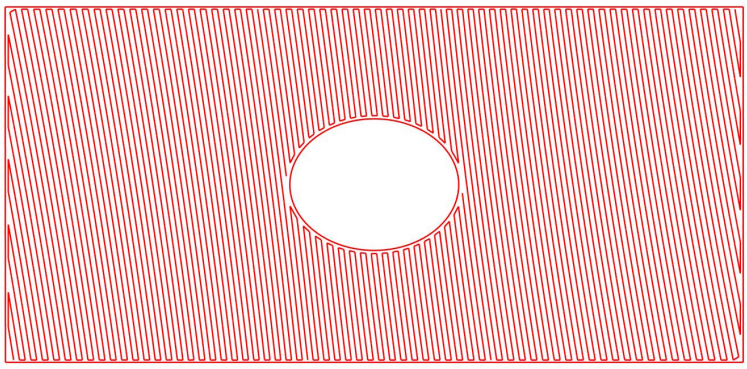

Figure 6.21: Strain Optimization for Curved fibers - Optimal Solution for the plate with hole: $w_{time} = 0.5$ and $w_{strain} = 0.5$.

the adaptability of the curved fibers to the hole, when using a stress based optimization.

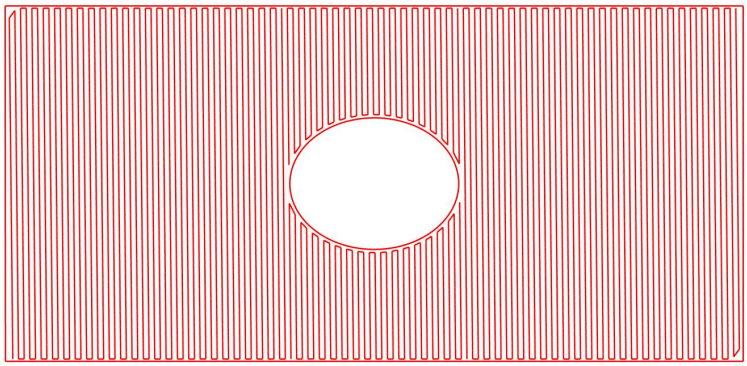

Figure 6.22: Strain Optimization for Curved fibers - Optimal Solution for the plate with hole: $w_{time} = 0$ and $w_{strain} = 1$.

6.4.2 Stress Optimization

6.4.2.1 Straight Fibers

Table 6.11: Optimal solutions for the plate with a hole for different weight combinations - Stress Optimization

Weight_Time	Weight_Stress	Theta (degrees)	Printing Time (s)	Stress
1	0	0	20995	1.143
0.5	0.5	31	21871	1.127
0	1	31	21871	1.127

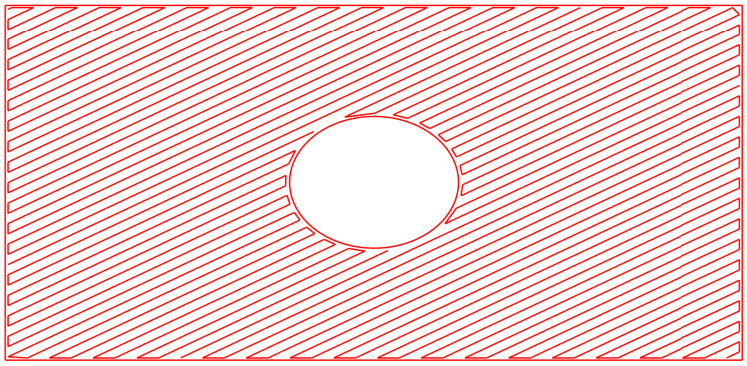

Figure 6.23: Stress Optimization for Straight fibers - Optimal Solution for the plate with a hole: $w_{time} = 0.5$ and $w_{stress} = 0.5$ & : $w_{time} = 0$ and $w_{stress} = 1$.

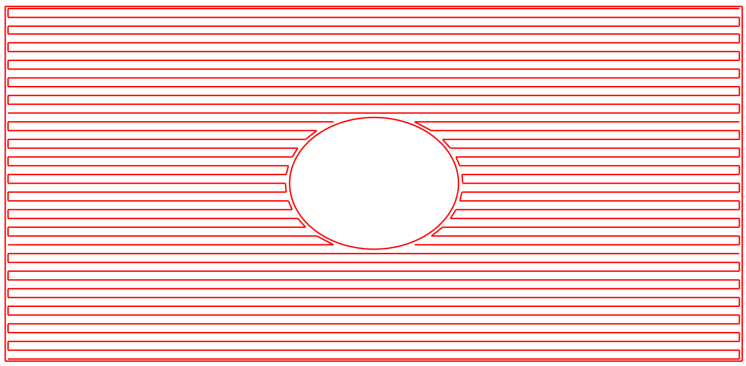

Figure 6.24: Stress Optimization for Straight fibers - Optimal Solution for the plate without a hole: $w_{time} = 1$ and $w_{strain} = 0$

6.4.2.2 Curved Fibers

Table 6.12: Optimal solutions for the plate with a hole for different weight combinations - Stress Optimization

Weight_Time	Weight_Stress	T_0 (rads)	T_1 (rads)	Phi (rads)
1	0	1.69	5.52	-3.79
0.5	0.5	44.3	0.39	-32.7
0	1	90	-89.9	-21.9

Table 6.13: Optimal solutions for the plate for different weight combinations

Weight_Time	Weight_Stress	Printing time (s)	Stress
1	0	20983	1.158
0.5	0.5	23086	1.141
0	1	30030	1.091

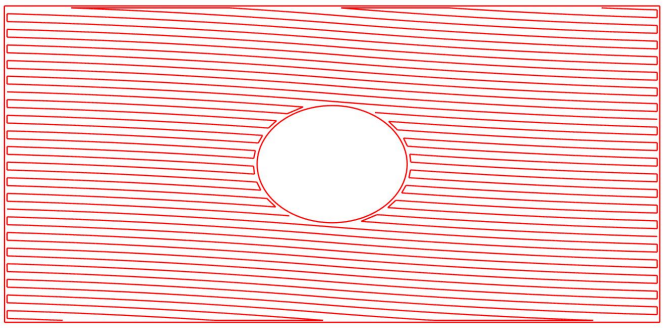

Figure 6.25: Stress Optimization for Curved fibers - Optimal Solution for the plate with a hole: $w_{time} = 1$ and $w_{stress} = 0$

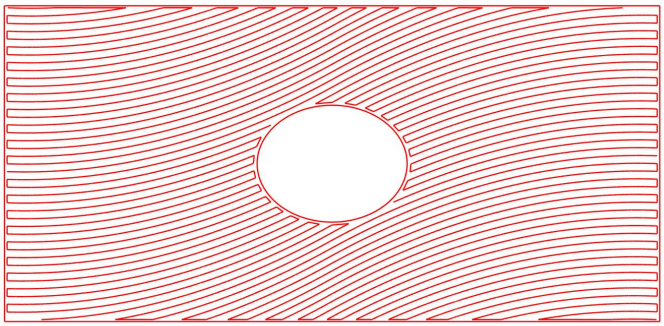

Figure 6.26: Stress Optimization for Curved fibers - Optimal Solution for the plate with a hole: $w_{time} = 0.5$ and $w_{stress} = 0.5$

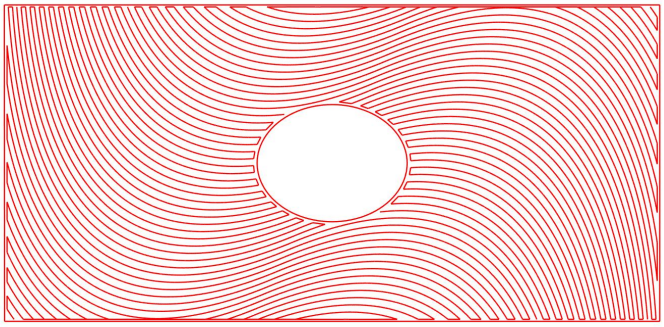

Figure 6.27: Stress Optimization for Curved fibers - Optimal Solution for the plate with a hole: $w_{time} = 0$ and $w_{stress} = 1$

As mentioned before, the results from this sections were supposed to be the most interesting ones. Again, when only time is considered, the result is similar to the previous ones introduced. When stress is taken into account, first with a weight of only 0.5, it is possible to observe that even though the orientation is similar to the straight case with the same weights, there is a tendency of the fibers to curve and to adapt to the hole. This fact is more noticeable when only the stress is considered, in figure 6.27. Once again, the printing times are higher, but the stress, especially for the case when $w_{stress} = 1$, is lower.

6.4.3 Parametric Study for Straight Fibers - Shell Plate with a hole

The same procedure was followed for this geometry.

The plots with the results are introduced below:

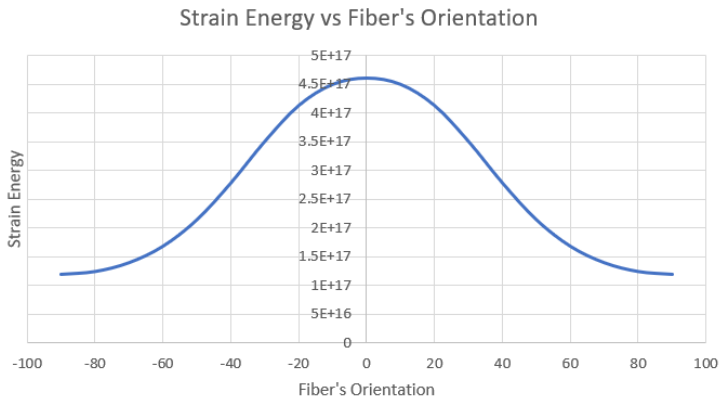

Figure 6.28: Parametric Study - Strain Energy

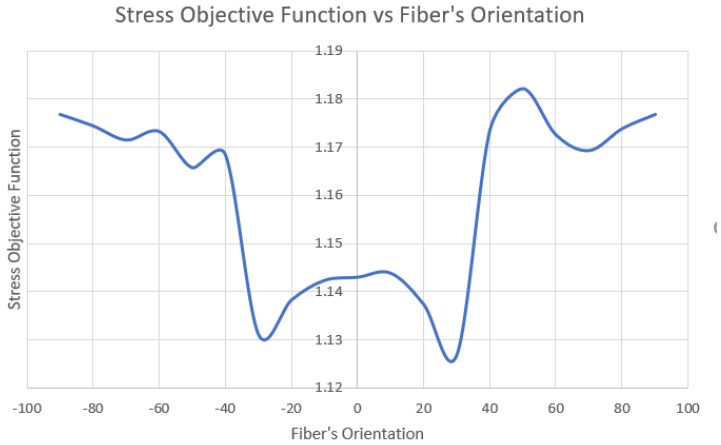

Figure 6.29: Parametric Study - Stress

For the first plot, the same results as the the previous geometry are obtained, the minimum strain energy occurs for 90 degrees, which is the result obtained through the optimization process. When it comes to the stress, the minimum is obtained exactly for 31 degrees, which is the same result as the one obtained in the optimization.

6.5 3D Analysis

In longitudinal tensile loading, the combination of compressive and tensile mode of failure occurs in three point bending i.e., the top surface of the layers will be subjected to compression mode and bottom surface of the layers submit to a state of tension. Therefore, examining the failure phenomenon in bending is more complex than in tension [81], and since the optimizations already take a long time to run, then the 3D specimen was only analyzed under traction.

Due to time limitations, only a stress optimization will be performed in this 3D specimen, for curved fibers. In order to be able to understand the quality of the results, it will be compared with a specimen with straight fibers aligned with the load.

6.5.1 Stress Optimization

This is an interesting case to use in a stress based optimization because the existence of a hole will contribute for a stress accumulation around it, and it will force the curved fibers to adapt around this feature. The optimal solution considering both weight factors equal to 0.5 is represented in the picture below:

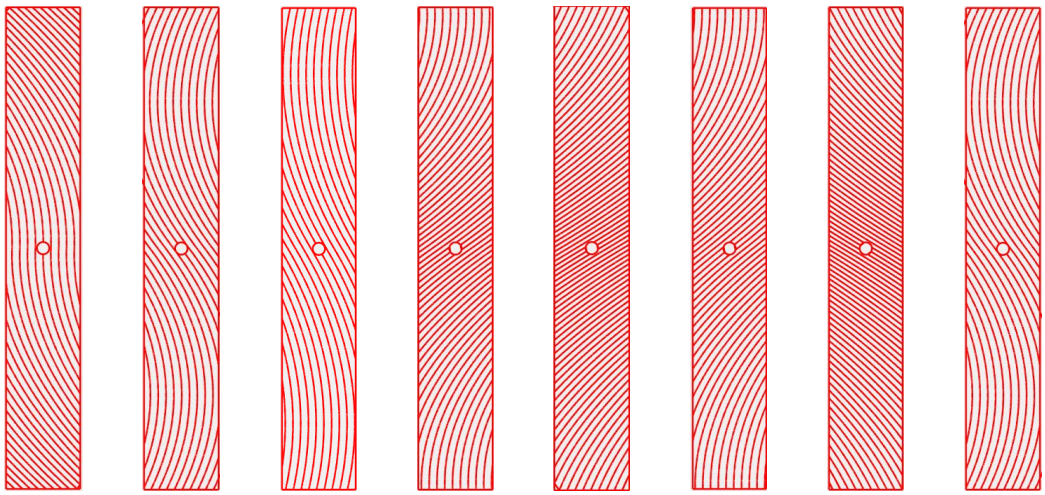

Figure 6.30: Stress Optimization for Curved fibers - Optimal Solution for plies of the specimen (from z=-0.508 to z=0.508), with $w_{time} = 0.5$ and $w_{stress} = 0.5$

For the final part, with the 8 layers combined, these are the final results:

- Printing time: 64222s;
- Stress: 1.15.

For the reference specimen, i.e. where all the fibers are alligned with the horizontal axis (0 degrees), these are the values of the stress and printing time:

- Printing time: 39016s;

– Stress: 1.21.

Again, and as expected, the printing time for curved fibers is considerably higher. However, the main goal of this case, since it is still in an early stage, was to verify that at both ends, the fibers tend to 0 degrees, which is the most logical orientation regarding the boundary conditions at both ends. Furthermore, around the holes, where there is concentration of stresses, it is possible to observe the curves adapting to it. This adaptation would increase if more design variables were to be considered. Finally, regarding the values of stress, they are similar, but with the additional design variables, the value for stress using VAT composites it is expected to decrease. Nonetheless, the value is still lower for the VAT composite.

Chapter 7

Conclusions and Future Work

In this chapter, the final considerations on the study are presented. The main achievements of the work are outlined and a note on the future work is given.

7.1 Achievements

The thesis research aimed at providing an optimization tool for CFRP composites to maximize the structural performance and minimizing printing time. For that end, a path plannning algorithm was successfully implemented in MATLAB, for both curved and straight fibers. Both optimizations were implemented for different case studies, and different and coherent results were obtained.

7.2 Conclusions

An optimization framework has been developed for 3D printers to integrate the structural and the manufacturing perspectives.

Firstly, the path planning algorithm was successfully implemented in order to determine the printing time of the different parts. Even though not a lot of information is available regarding this matter, some values present in the literature were used, and adapted for the printing of the curved fibers model. Furthermore, this path planning and the computation of the printing time is adaptable to every printer, as long as the information regarding the maximum and minimum velocity, the acceleration and the nozzle diameter is provided.

Regarding the optimization, first, a framework of structural optimization was developed where the printing time was integrated. Second, the framework itself is also easily adaptable to other printers and also to other objective functions. Moreover, and focusing now in the results, when only the time is considered, all the 2D models presented similar results. This is the first proof that the optimizer was working correctly. Since the geometries were very similar it would not make sense

to have differences in the final design. Still considering the time, it has to be taken into account that only 1 ply is considered in this study. When the full model, with several plies, is contemplated, then the time difference is considerable. In addition, when the geometry with a hole is considered, it is possible to observe the adaptation of the curves around the hole, where the stresses are concentrated. This is another evidence of the success of the implementation of this framework.

Regarding the 3D specimen, this case study was not explored to its fullest, largely due to the amount of time needed to run the simulations, but also because it was not a priority goal of this work. However, it was also possible to observe curved adapting around the hole. For this case, it would also make sense to increase the number of design variables, in order to increase the freedom of design.

7.3 Future Work

Even though some interesting results were achieved, a lot of research still needs to be done in this field, in order to determine the best designs and the properties of the CFRP composites manufactured using AM.

Regarding the work presented, the next steps are the completion of the analysis of the 3D specimen, with a larger number of design variables.

Furthermore, the implementation of the path planning in a 3D printer in order to produce parts and to perform an experimental analysis, so that the results could be confirmed.

Another suggestion for further work in the matter is to consider different objective functions. In this work, besides strain and stress optimization, the printing time was also optimized. However, other parameters, equal or more important, could also be considered, such as: material cost and printing restrictions. The latter is particularly interesting and important, since the manufacturing process of VAT composites is highly complex.

A final suggestion for future work is to perform optimizations in more complex geometries.

Bibliography

[1] Carter WT, Erno DJ, Abbott DH, Bruck CE, Wilson GH, Wolfe JB, Finkhousen DM, Tepper A, Stevens RG. The GE aircraft engine bracket challenge: an experiment in crowdsourcing for mechanical design concepts. In25th Annual International Solid Freeform Fabrication Symposium, Austin, TX, Aug 2014 (pp. 4-6).

[2] Ferguson I. Using Topology Optimization to Improve Design for Additive Manufacture.

[3] Rodríguez JF, Thomas JP, Renaud JE. Mechanical behavior of acrylonitrile butadiene styrene fused deposition materials modeling. Rapid Prototyping Journal. 2003 Oct 1;9(4):219-30.

[4] Ning F, Cong W, Wei J, Wang S, Zhang M. Additive manufacturing of CFRP composites using fused deposition modeling: effects of carbon fiber content and length. InASME 2015 International Manufacturing Science and Engineering Conference 2015 Jun 8. American Society of Mechanical Engineers Digital Collection.

[5] Nebelsick JH, Allgaier C, Felbrich B, Coupek D, Reiter R, Reiter G, Menges A, Lechler A, Wurst KH. Continuous Fused Deposition Modelling of Architectural Envelopes Based on the Shell Formation of Molluscs: A Research Review. InBiomimetic Research for Architecture and Building Construction 2016 (pp. 243-260). Springer, Cham.

[6] Todoroki A, Watanabe K, Kobayashi H. Application of genetic algorithms to stiffness optimization of laminated composite plates with stress-concentrated open holes. JSME Int J 1995;38(4):458–64.

[7] Adams DB, Watson LT, Gurdal Z, Anderson-Cook CM. Genetic algorithm optimization and blending of composite laminates by locally reducing laminate thickness. Adv Eng Soft 2004;35:35–43.

[8] Kang JH, Kim CG. Minimum weight design of compressively loaded composite plates and stiffened panels for post-buckling strength by genetic algorithm. Compos Struct 2005;69:239–46.

[9] ASTM COMMITTEE F42 ON ADDITIVE MANUFACTURING TECHNOLOGIES; ASTM COMMITTEE F42 ON ADDITIVE MANUFACTURING TECHNOLOGIES. SUBCOMMITTEE

F42. 91 ON TERMINOLOGY. Standard terminology for additive manufacturing technologies. ASTM International, 2012.

[10] Weller C, Kleer R, Piller FT. Economic implications of 3D printing: Market structure models in light of additive manufacturing revisited. International Journal of Production Economics. 2015 Jun 1;164:43-56.

[11] Lyons B. Additive manufacturing in aerospace: Examples and research outlook. The Bridge. 2014;44(3).

[12] https://www.boeing.com/features/innovation-quarterly/nov2017/feature-thought-leadership-3d-printing.page Retrieved August 2, 2019

[13] ASTM COMMITTEE F42 ON ADDITIVE MANUFACTURING TECHNOLOGIES; ASTM COMMITTEE F42 ON ADDITIVE MANUFACTURING TECHNOLOGIES. SUBCOMMITTEE F42. 91 ON TERMINOLOGY. Standard terminology for additive manufacturing technologies. ASTM International, 2012.

[14] Pedersen DB, De Chiffre L, Hansen HN. Additive manufacturing: multi material processing and part quality control.

[15] Dong G, Tang Y, Li D, Zhao YF. Mechanical Properties of Continuous Kevlar Fiber Reinforced Composites Fabricated by Fused Deposition Modeling Process. Procedia Manufacturing. 2018 Jan 1;26:774-81.

[16] Wendel B, Rietzel D, Kühnlein F, Feulner R, Hülder G, Schmachtenberg E. Additive processing of polymers. Macromolecular materials and engineering. 2008 Oct 10;293(10):799-809.

[17] Gao W, Zhang Y, Ramanujan D, Ramani K, Chen Y, Williams CB, Wang CC, Shin YC, Zhang S, Zavattieri PD. The status, challenges, and future of additive manufacturing in engineering. Computer-Aided Design. 2015 Dec 1;69:65-89.

[18] Sharma A. A computational approach to achieve uniform mechanical properties along the built-up direction in WAAM component (Doctoral dissertation, Indian institute of technology Hyderabad).

[19] Sealy MP, Madireddy G, Williams RE, Rao P, Toursangsaraki M. Hybrid processes in additive manufacturing. Journal of Manufacturing Science and Engineering. 2018 Jun 1;140(6):060801.

[20] Wahlström T, Sahlström J. Additive Manufacturing in Production-for the Automotive Industry.

[21] Pham DT, Gault RS (1998) A comparison of rapid prototyping technologies. Int J Mach Tools Manuf 38(10):1257–1287.

[22] Ding Y, Lan H, Hong J, Wu D. An integrated manufacturing system for rapid tooling based on rapid prototyping. Robotics and computer-integrated manufacturing. 2004 Aug 1;20(4):281-8.

[23] Gebhardt A. Rapid Prototyping–Rapid Tooling–Rapid Manufacturing. Carl Hanser, München. 2007.

[24] Wang YC, Chen T, Yeh YL. Advanced 3D printing technologies for the aircraft industry: a fuzzy systematic approach for assessing the critical factors. The International Journal of Advanced Manufacturing Technology. 2018:1-1.

[25] Aston R (2017) 3D printing done right - Applying additive manufacturing in integrated mechanical designs. https://www.boeing.com/features/innovation-quarterly/nov2017/feature-thought-leadership-3d-printing.page, Retrieved August 28, 2019

[26] ”Next 3-D Frontier: Printed Plane Parts”, Wall Street Journal, July 2014, 2012.

[27] European Space Agency investigates Additive Manufacturing DMP parts for inspace satellite engines. (2015, March). Retrieved August 29, 2019, from www.3dsystems.com/learning-center/case-studies/european-space-agencyinvestigates-additive-manufacturing-dmp-parts

[28] https://www.ge.com/additive/blog/new-manufacturing-milestone-30000-additive-fuel-nozzles Retrieved September 3, 2019

[29] KELLNER, Thomas. An Epiphany Of Disruption: GE Additive Chief Explains How 3D Printing Will Upend Manufacturing. GE Reports, November, 2017, 19.

[30] Scott Crump, “US5121329 A - Apparatus and method for creating three-dimensional objects,” 1992.

[31] Singh R, Singh S, Singh IP, Fabbrocino F, Fraternali F. Investigation for surface finish improvement of FDM parts by vapor smoothing process. Composites Part B: Engineering. 2017 Feb 15;111:228-34.

[32] dos Santos JA. Additive manufacturing of thermoplastic matrix composites.

[33] Ning F, Cong W, Qiu J, Wei J, Wang S. Additive manufacturing of carbon fiber reinforced thermoplastic composites using fused deposition modeling. Composites Part B: Engineering. 2015 Oct 1;80:369-78.

[34] Jerez-Mesa R, Gomez-Gras G, Travieso-Rodriguez JA, Garcia-Plana V. A comparative study of the thermal behavior of three different 3D printer liquefiers. Mechatronics. 2018 Dec 1;56:297-305.

[35] Swanson WJ, Hopkins PE, inventors; Stratasys Inc, assignee. Thin-wall tube liquifier. United States patent US 6,004,124. 1999 Dec 21.

[36] Swanson WJ, Schloesser RG, Larson G, inventors; Stratasys Inc, assignee. Additive manufacturing method for printing three-dimensional parts with purge towers. United States patent US 9,421,713. 2016 Aug 23.

[37] Swanson WJ, Turley PW, Leavitt PJ, Karwoski PJ, LaBossiere JE, Skubic RL, inventors; Stratasys Inc, assignee. High temperature modeling apparatus. United States patent US 6,722,872. 2004 Apr 20.

[38] Dudek PF. FDM 3D printing technology in manufacturing composite elements. Archives of Metallurgy and Materials. 2013 Dec 1;58(4):1415-8.

[39] Novakova-Marcincinova L, Novak-Marcincin J, Barna J, Torok J. Special materials used in FDM rapid prototyping technology application. In2012 IEEE 16th International Conference on Intelligent Engineering Systems (INES) 2012 Jun 13 (pp. 73-76). IEEE.

[40] Lauke B, Fu SY. Strength anisotropy of misaligned short-fibre-reinforced polymers. Composites Science and Technology. 1999 Apr 1;59(5):699-708.

[41] Fu SY, Hu X, Yue CY. Effects of fiber length and orientation distributions on the mechanical properties of short-fiber-reinforced polymers. Journal of the Society of Materials Science, Japan. 1999 Jun 15;48(6Appendix):74-83.

[42] Friedrich K, Almajid AA. Manufacturing aspects of advanced polymer composites for automotive applications. Applied Composite Materials. 2013 Apr 1;20(2):107-28.

[43] Matsuzaki R, Ueda M, Namiki M, Jeong TK, Asahara H, Horiguchi K, Nakamura T, Todoroki A, Hirano Y. Three-dimensional printing of continuous-fiber composites by in-nozzle impregnation. Scientific reports. 2016 Mar 11;6:23058.

[44] Van Der Klift F, Koga Y, Todoroki A, Ueda M, Hirano Y, Matsuzaki R. 3D printing of continuous carbon fibre reinforced thermo-plastic (CFRTP) tensile test specimens. Open J. Compos. Mater. 2016 Jan;6(1):18-27.

[45] Li N, Li Y, Liu S. Rapid prototyping of continuous carbon fiber reinforced polylactic acid composites by 3D printing. Journal of Materials Processing Technology. 2016 Dec 1;238:218-25.

[46] Nakagawa Y, Mori KI, Maeno T. 3D printing of carbon fibre-reinforced plastic parts. The International Journal of Advanced Manufacturing Technology. 2017 Jul 1;91(5-8):2811-7.

[47] Vaneker TH. Material extrusion of continuous fiber reinforced plastics using commingled yarn. Procedia CIRP. 2017 Jan 1;66:317-22.

[48] Yamawaki M, Kouno Y. Fabrication and mechanical characterization of continuous carbon fiber-reinforced thermoplastic using a preform by three-dimensional printing and via hot-press molding. Advanced Composite Materials. 2018 Mar 4;27(2):209-19.

[49] Catapano A, Montemurro M, Balcou JA, Panettieri E. Rapid Prototyping of Variable Angle-Tow Composites. Aerotecnica Missili Spazio. 2019 Dec 1;98(4):257-71.

[50] Kim BC, Potter K, Weaver PM. Continuous tow shearing for manufacturing variable angle tow composites. Composites Part A: Applied Science and Manufacturing. 2012 Aug 1;43(8):1347-56.

[51] Weaver P, Potter K, Hazra K, Saverymuthapulle M, Hawthorne M. Buckling of variable angle tow plates: from concept to experiment. In50th AIAA/ASME/ASCE/AHS/ASC structures, structural dynamics, and materials conference 17th AIAA/ASME/AHS adaptive structures conference 11th AIAA No 2009 (p. 2509).

[52] Blom AW, Abdalla MM, Gürdal Z. Optimization of course locations in fiber-placed panels for general fiber angle distributions. Composites Science and Technology. 2010 Apr 1;70(4):564-70.

[53] Ding D, Pan Z, Cuiuri D, Li H, van Duin S. Advanced design for additive manufacturing: 3D slicing and 2D path planning. New Trends in 3D Printing. 2016 Jul 13.

[54] Dunlavey MR. Efficient polygon-filling algorithms for raster displays. ACM Transactions on Graphics (TOG). 1983 Oct 1;2(4):264-73.

[55] Zhang Y, Chen Y, Li P, Male AT. Weld deposition-based rapid prototyping: a preliminary study. Journal of Materials Processing Technology. 2003 Apr 20;135(2-3):347-57.

[56] Bertoldi M, Yardimci M, Pistor CM, Guceri SI. Domain decomposition and space filling curves in toolpath planning and generation. In1998 International Solid Freeform Fabrication Symposium 1998.

[57] Wasser T, Jayal AD, Pistor C. Implementation and evaluation of novel buildstyles in fused deposition modeling (FDM). In1999 International Solid Freeform Fabrication Symposium 1999.

[58] Jenkins WM. Towards structural optimization via the genetic algorithm. Computers & Structures. 1991 Jan 1;40(5):1321-7.

[59] Goldberg DE. Genetic Algorithms in Search, Optimization, and Machine Learning, Addison Wesley, Reading, MA. SUMMARY THE APPLICATIONS OF GA-GENETIC ALGORITHM FOR DEALING WITH SOME OPTIMAL CALCULATIONS IN ECONOMICS. 1989.

[60] Marín, L., Trias, D., Badalló, P., Rus, G., & Mayugo, J. A. (2012). Optimization of composite stiffened panels under mechanical and hygrothermal loads using neural networks and genetic algorithms. Composite structures, 94: 3321-3326.

[61] Le Riche, R., & Haftka, R. T. (1993). Optimization of laminate stacking sequence for buckling load maximization by genetic algorithm. AIAA journal, 31, 951-956.

[62] Escusa GG, Sena-Cruz J, Cruz F, Pereira EN, Valente IB, Barros JA. The use of genetic algorithms for structural optimization of hybrid sandwich panels. InAPFIS2017-6th Asia-Pacific Conference on FRP in Structures 2017 Jul 19 (pp. 1-5).

[63] Wang H, Stori JA. A metric-based approach to 2D tool-path optimization for high-speed machining. InASME 2002 International Mechanical Engineering Congress and Exposition 2002 Jan 1 (pp. 139-148). American Society of Mechanical Engineers.

[64] http://dsk.ippt.pan.pl/docs/abaqus/v6.13/index.html Retrieved August 15, 2019

[65] ABAQUS, Abaqus Documentation. Version 6.13. 2014. Dassault Systemes: 3DS Paris Campus, 10.

[66] Puri G. Python scripts for Abaqus: learn by example. Gautam Puri; 2011.

[67] Weicker K, Weicker N. Basic principles for understanding evolutionary algorithms. Fundamenta Informaticae. 2003 Jan 1;55(3-4):387-403.

[68] Pengfei G, Xuezhi W, Yingshi H. An Imitative Full Stress Genetic Algorithm for Structural Optimization with Discrete Variables. In2009 WRI Global Congress on Intelligent Systems 2009 May 19 (Vol. 1, pp. 579-583). IEEE.

[69] Janjić A, Velimirović L, Stanković M. Multi-attribute Optimization of Electric Vehicle Fleet Charging Scheduling. InBOOK OF ABSTRACTS 2005 (Vol. 144, No. 1, p. 4).

[70] https://markforged.com/mark-two/ Retrieved August 28, 2019

[71] Melenka GW, Cheung BK, Schofield JS, Dawson MR, Carey JP. Evaluation and prediction of the tensile properties of continuous fiber-reinforced 3D printed structures. Composite Structures. 2016 Oct 1;153:866-75.

[72] Sauer MJ. Evaluation of the mechanical properties of 3D printed carbon fiber composites (Doctoral dissertation, Mechanical Engineering Department, South Dakota State University).

[73] Chamis CC. Simplified composite micromechanics equations for hygral, thermal and mechanical properties.

[74] Asif S. Modelling and path planning for additive manufacturing of continuous fiber composites (Doctoral dissertation).

[75] Jin GQ, Li WD, Gao L, Popplewell K. A hybrid and adaptive tool-path generation approach of rapid prototyping and manufacturing for biomedical models. Computers in industry. 2013 Apr 1;64(3):336-49.

[76] Ahmad Z, Zoppi M, Molfino R. Fixture Layout Optimization Using Element Strain Energy and Genetic Algorithm. World Academy of Science, Engineering and Technology, International Journal of Mechanical, Aerospace, Industrial, Mechatronic and Manufacturing Engineering. 2013 Sep 1;7(10):1924-30.

[77] Yang RJ, Chen CJ. Stress-based topology optimization. Structural optimization. 1996 Oct 1;12(2-3):98-105.

[78] Jeyakodi GT. Finite element simulation of the in-situ AFP process for thermoplastic composites using Abaqus.

[79] Catapano A, Montemurro M. A multi-scale approach for the optimum design of sandwich plates with honeycomb core. Part II: the optimisation strategy. Composite structures. 2014 Dec 1;118:677-90.

[80] Montemurro M, Catapano A, Doroszewski D. A multi-scale approach for the simultaneous shape and material optimisation of sandwich panels with cellular core. Composites Part B: Engineering. 2016 Apr 15;91:458-72.

[81] Naresh K, Krishnapillai S, Velmurugan R. Effect of fiber orientation on carbon/epoxy and glass/epoxy composites subjected to shear and bending. InSolid State Phenomena 2017 (Vol. 267, pp. 103-108). Trans Tech Publications.

[82] Norman DA, Robertson RE. The effect of fiber orientation on the toughening of short fiber-reinforced polymers. Journal of applied polymer science. 2003 Dec 5;90(10):2740-51.

Appendix A

Genetic Algorithm

A.0.0.1 Data Structures

This structure stores an entire population in a single matrix of size Nind x Lind, being Nind the number of individuals in the population and Lind the length of the genotypic representation of those individuals. Each row corresponds to an individual's genotype, consisting of base-n, typically binary, values:

$$Chrom = \begin{bmatrix} g_{(1,1)} & g_{(1,2)} & g_{(1,3)} & \cdots & g_{(1,L_{ind})} \\ g_{(2,1)} & g_{(2,2)} & g_{(2,3)} & \cdots & g_{(2,L_{ind})} \\ g_{(3,1)} & g_{(3,2)} & g_{(3,3)} & \cdots & g_{(3,L_{ind})} \\ . & . & . & \cdots & . \\ g_{(N_{ind},1)} & g_{(N_{ind},2)} & g_{(N_{ind},3)} & \cdots & g_{(N_{ind},L_{Lind})} \end{bmatrix}$$

This data representation only requires that all chromossomes are of equal length. Thus, structured population or populations with varying genotypic bases may be used in the GA Toolbox provided that a suitable decoding function is employed when mapping chromossomes onto phenotypes.

A.0.0.2 Phenotypes

Phenotypes, also known as decision variables, are obtained by applying some mapping from chromossome representation into the decision variable space. Here, each string contained in the chromossome structure decodes to a row vector of order Nvar, according to the number of dimensions in the search space and corresponding to the decision variable vector value [69]. The phenotypes are stored in a numerical matrix of size Nind x Nvar. In the same line of thought, each row corresponds to a particular individual's phenotype. An example is given below of the phenotype data structure, where *bin2real* is used to represent an arbitrary function mapping the genotypes onto the phenotypes.

```
Phen = bin2real(Chrom) \% map genotype to phenotype
```

$$Chrom = \begin{bmatrix} x_{(1,1)} & x_{(1,2)} & x_{(1,3)} & \cdots & x_{(1,N_{var})} \\ x_{(2,1)} & x_{(2,2)} & x_{(2,3)} & \cdots & x_{(2,N_{var})} \\ x_{(3,1)} & x_{(3,2)} & x_{(3,3)} & \cdots & x_{(3,N_{var})} \\ . & . & . & \cdots & . \\ x_{(N_{ind},1)} & x_{(N_{ind},2)} & x_{(N_{ind},3)} & \cdots & x_{(N_{ind},N_{var})} \end{bmatrix}$$

The actual mapping between the chromossome representation and their phenotypic values depends upon the bin2real function used. Having this, it is perfectly possible to have vectors of decision variables of different types, e.g. it is possible to mix integer, real-value and binary decision variables in the same Phen data structure.

A.0.0.3 Objective Function Values

The objective function is used in order to evaluate the performance of the decision variables in the problem domain. Objective functions can either be scalar or vectorial, as it is the case of multi-objective problems. Important to highlight that objective function values are not necessarily the same as the fitness values [69]. The values of the objective function are stored in a numerical matrix of size Nind x Nobj, where the later is the number of objectives. Each row corresponds, once again, to a specific individual's objective vector.

```
Objv = OBJFUN(Phen) \% Objective Function
```

$$Chrom = \begin{bmatrix} y_{(1,1)} & y_{(1,2)} & y_{(1,3)} & \cdots & y_{(1,N_{var})} \\ y_{(2,1)} & y_{(2,2)} & y_{(2,3)} & \cdots & y_{(2,N_{var})} \\ y_{(3,1)} & y_{(3,2)} & y_{(3,3)} & \cdots & y_{(3,N_{var})} \\ . & . & . & \cdots & . \\ y_{(N_{ind},1)} & y_{(N_{ind},2)} & y_{(N_{ind},3)} & \cdots & y_{(N_{ind},N_{var})} \end{bmatrix}$$

A.0.0.4 Fitness Values

Fitness valued are obtained from the objective function values through a scalling or ranking function. Fitness values are non-negative scalars and are stored in column vectors of length Nind. An example is given below:

```
Fitn= ranking(ObjV) \% Fitness Function
```

$$Fitn = \begin{matrix} f_1 \\ y_2 \\ y_3 \\ ... \\ f_{N_{ind}} \end{matrix}$$

A.0.0.5 Toolbox Functions

In order to call the function at the command line, the syntax used is:

```
[x fval] = ga(@fitnessfun, nvars, options)
```

where

- @fitnessfun is a handle to the fitness function;
- nvars is the number of independent variables for the fitness function;
- options is a structure containing options for the genetic algorithm. If you do not pass in this argument, 'ga' uses its default options.

When it comes to the results:

- x is the point at which the final value is atained;
- fval is the final value of the fitness function.

A.0.0.6 Results

Two different values are plot after each generation, 'Best Fitness' and 'Mean Fitness'. Best fitness represents the best design within the number of individuals, part of each generation. On the other hand, the mean fitness is the average value of the individuals in each generation.

An example of a GA's plot in MatLab is introduced in the next figure, where the best fitness is plotted in black and the mean fitness is plotted in blue:

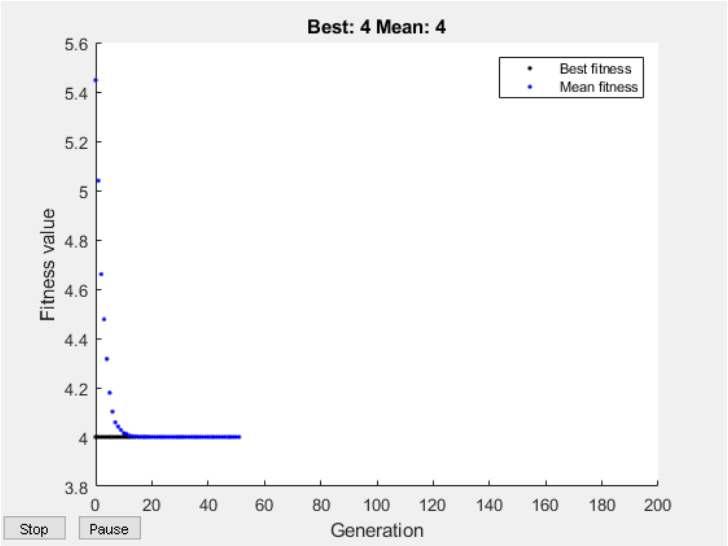

Figure A.1: GA's plot in MATLAB

Appendix B

Compliance Matrix

$$\bar{S}_{11} = S_{11}cos^4\theta - 2S_{16}cos^3\theta sin\theta + (2S_{12} + S_{66})cos^2\theta sin^2\theta - 2S_{26}cos\theta sin^3\theta + S_{22}sin^4\theta$$

$$\bar{S}_{12} = S_{12}cos^4\theta + (S_{16} + S_{26})cos^3\theta sin\theta + (S_{11} + S_{22} - S_{66})cos^2\theta sin^2\theta + (S_{26} - S_{16})cos\theta sin^3\theta + S_{12}sin^4\theta$$

$$\bar{S}_{13} = S_{13}cos^2\theta - S_{36}cos\theta sin\theta + S_{23}sin^2\theta$$

$$\bar{S}_{16} = S_{16}cos^4\theta + (2S_{11} - 2S_{12} - S_{66})cos^3\theta sin\theta + 3(S_{26} - S_{16})cos^2\theta sin^2\theta + (S_{66} + 2S_{12} - 2S_{22})cos\theta sin^3\theta - S_{26}sin$$

$$\bar{S}_{22} = S_{22}cos^4\theta + S_{26}cos^3\theta sin\theta + (2S_{12} + S_{66})cos^2\theta sin^2\theta + 2S_{16}cos\theta sin^3\theta + S_{11}sin^4\theta$$

$$\bar{S}_{23} = S_{23}cos^2\theta + S_{36}cos\theta sin\theta + S_{13}sin^2\theta$$

$$\bar{S}_{26} = S_{26}cos^4\theta + (2S_{12} - S_{22} + S_{66})S_{36}cos^3\theta sin\theta + 3(S_{16} - S_{26})cos^2\theta sin^2\theta + 2(2S_{11} - S_{12} - S_{66})cos\theta sin^3\theta - S_{16}s$$

$$\bar{S}_{33} = S_{33}$$

$$\bar{S}_{36} = 2(S_{13} - S_{23})cos\theta sin + S_{36}(cos^2\theta - sin^2\theta)$$

$$\bar{S}_{66} = S_{66}(cos^2\theta - sin^2\theta)^2 + 4(S_{16} - S_{26})(cos^2\theta - sin^2\theta)cos\theta sin\theta + 4(S_{11} + S_{22} - 2S_{12})cos^2\theta sin^2\theta$$

$$\bar{S}_{44} = S_{44}cos^2\theta + 2S_{45}cos\theta sin\theta + S_{55}sin^2\theta$$

$$\bar{S}_{45} = S_{45}(cos^2\theta - sin^2\theta) + (S_{55} - S_{44})$$

$$\bar{S}_{55} = S_{55}cos^2\theta + S_{44}sin^2\theta - S_{45}cos\theta sin\theta$$

$$\bar{S}_{14} = S_{14}cos^3\theta + (S_{15} - S_{46})cos^2\theta sin\theta$$

$$\bar{S}_{15} = S_{15}cos^3\theta - (S_{14} + S_{56})cos^2\theta sin\theta + (S_{25} + S_{46})cos\theta sin^2\theta - S_{24}sin^3\theta$$

$$\bar{S}_{24} = S_{24}cos^3\theta + (S_{25} + S_{46})cos^2\theta sin\theta + (S_{14} + S_{56})cos\theta sin^2\theta + S_{15}sin^3\theta$$

$$\bar{S}_{25} = S_{25}cos^3\theta + (-S_{24} + S_{56})cos^2\theta sin\theta + (S_{15} - S_{46})cos\theta sin^2\theta - S_{14}sin^3\theta$$

$$\bar{S}_{34} = S_{34}cos\theta + S_{35}sin\theta$$

$$\bar{S}_{35} = S_{35}cos\theta - S_{34}sin\theta$$

$$\bar{S}_{46} = (2S_{14} - 2S_{24} + S_{56})cos^2\theta sin\theta + (2S_{15} - 2S_{25} - S_{46})cos^2\theta sin^2\theta + S_{46}cos^3\theta - S_{56}sin^3\theta$$

$$\bar{S}_{56} = (2S_{15} - 2S_{25} + S_{46})cos^2\theta sin\theta + (2S_{24} - 2S_{14} - S_{56})cos^2\theta sin^2\theta + S_{56}cos^3\theta + S_{46}sin^3\theta$$

(B.1)

Appendix C

Code

In the code, 'DMO Plate' is the name of the model, 'Plate' the name of the part and k is the variable that identifies the number of the element.

C.0.0.0.1 Determination of the coordinates of one vertice

```
connectivity=mdb.models['DMO Plate'].parts['Plate'].elements[k].connectivity
e0=connectivity[0]
coord_x_0=mdb.models['DMO Plate'].rootAssembly.instances['plateInstance'].nodes[e0].coordinates
coord_y_0=mdb.models['DMO Plate'].rootAssembly.instances['plateInstance'].nodes[e0].coordinates
```

C.0.0.0.2 Determination of the center of one triangle

```
iX=(coord_x_0 + coord_x_1 + coord_x_2)/3
iY=(coord_y_0 + coord_y_1 + coord_y_2)/3
```

C.0.0.0.3 Determination of the intersection of the diagonals of the quadrilateral

```
line1=((iX,iY),(jX,jY))
line2=((kX,kY),(lX,lY))

xdiff = (line1[0][0] - line1[1][0], line2[0][0] - line2[1][0])
ydiff = (line1[0][1] - line1[1][1], line2[0][1] - line2[1][1])

def det(a, b):
    return a[0] * b[1] - a[1] * b[0]

div = det(xdiff, ydiff)
```

```
if div == 0:
    raise Exception('lines do not intersect')

d = (det(*line1), det(*line2))

xc = det(d, xdiff) / div
yc = det(d, ydiff) / div
```

C.0.0.0.4 Crash Code

```
    if crash==1

    IniDes=dlmread('C:\3d\PopulationDesign.txt');
    opts=optimoptions('ga','OutputFcn',@output_3d,'InitialPopulation',IniDes);
    opts=optimoptions(opts,'PopulationSize',30,'MaxGeneration',100,'PlotFcns',@gaplotbestf);

else
    opts=optimoptions('ga','OutputFcn',@output_3d);
    opts=optimoptions(opts,'PopulationSize',30,'MaxGeneration',100,'PopInitRange',[],'PlotFcns',
end
```